







# An organoid-derived bronchioalveolar model for SARS-CoV-2 infection of human alveolar type II-like cells

Mart M Lamers<sup>1,†</sup> , Jelte van der Vaart<sup>2,†</sup> , Kèvin Knoops<sup>3</sup>, Samra Riesebosch<sup>1</sup>, Tim I Breugem<sup>1</sup>, Anna Z Mykityn<sup>1</sup>, Joep Beumer<sup>2</sup> , Debby Schipper<sup>1</sup>, Karel Bezstarosti<sup>4</sup>, Charlotte D Koopman<sup>5</sup>, Nathalie Groen<sup>5</sup>, Raimond B G Ravelli<sup>3</sup>, Hans Q Duimel<sup>3</sup>, Jeroen A A Demmers<sup>4</sup>, Georges M G M Verjans<sup>1</sup> , Marion P G Koopmans<sup>1</sup>, Mauro J Muraro<sup>5</sup>, Peter J Peters<sup>3</sup>, Hans Clevers<sup>2,\*,‡</sup> & Bart L Haagmans<sup>1,\*,‡</sup> 

## Abstract

Severe acute respiratory syndrome coronavirus 2 (SARS-CoV-2) causes coronavirus disease 2019 (COVID-19), which may result in acute respiratory distress syndrome (ARDS), multiorgan failure, and death. The alveolar epithelium is a major target of the virus, but representative models to study virus host interactions in more detail are currently lacking. Here, we describe a human 2D air–liquid interface culture system which was characterized by confocal and electron microscopy and single-cell mRNA expression analysis. In this model, alveolar cells, but also basal cells and rare neuroendocrine cells, are grown from 3D self-renewing fetal lung bud tip organoids. These cultures were readily infected by SARS-CoV-2 with mainly surfactant protein C-positive alveolar type II-like cells being targeted. Consequently, significant viral titers were detected and mRNA expression analysis revealed induction of type I/III interferon response program. Treatment of these cultures with a low dose of interferon lambda 1 reduced viral replication. Hence, these cultures represent an experimental model for SARS-CoV-2 infection and can be applied for drug screens.

**Keywords** airway organoids; bronchioalveolar-like; COVID-19; pneumocytes; SARS-CoV-2

**Subject Categories** Methods & Resources; Microbiology, Virology & Host Pathogen Interaction; Respiratory System

**DOI** 10.15252/embj.2020105912 | Received 12 June 2020 | Revised 3 December 2020 | Accepted 4 December 2020

**The EMBO Journal (2021) e105912**

## Introduction

The severe acute respiratory syndrome coronavirus 2 (SARS-CoV-2) has spread globally within several months after an initial outbreak in Wuhan, China, in December 2019 (Zhu *et al.*, 2020). The World Health Organization (WHO) declared SARS-CoV-2 a pandemic on March 11, 2020. As of November 1, 2020, > 46,000,000 patients were confirmed including > 1,200,000 deaths (WHO, 2020). SARS-CoV-2 belongs to the Sarbecovirus subgenus (genus Betacoronavirus, family Coronaviridae), together with SARS-CoV (Andersen *et al.*, 2020; Coronaviridae Study Group of the International Committee on Taxonomy of V, 2020; Lu *et al.*, 2020). SARS-CoV-2 causes coronavirus disease 2019 (COVID-19), an influenza-like illness associated with a broad spectrum of clinical respiratory syndromes, ranging from mild upper airway symptoms to a life-threatening viral pneumonia (Chen *et al.*, 2020; Wang *et al.*, 2020; Wolfel *et al.*, 2020; Xu *et al.*, 2020). This pneumonia fulfills the radiographic and histological criteria for acute respiratory distress syndrome (ARDS). Classically, ARDS is caused by damage to the alveoli, more specifically to the alveolar type I cells that are critical in the oxygen transport from the alveoli to the blood, triggered through an inflammatory response to pathogens or toxins (Ware & Matthay, 2000; Thompson *et al.*, 2017; Ackermann *et al.*, 2020; Barton *et al.*, 2020; Menter *et al.*, 2020; Raptis *et al.*, 2020).

The early events that lead to respiratory failure as a result of coronavirus infection are initiated following virus replication (tenOever, 2016). After virus entry, which is determined by receptor availability, viral replication generates pathogen-associated molecular patterns, specifically RNA structures, that can be

<sup>1</sup> Viroscience Department, Erasmus University Medical Center, Rotterdam, The Netherlands

<sup>2</sup> Oncode Institute, Hubrecht Institute, Royal Netherlands Academy of Arts and Sciences and University Medical Center, Utrecht, The Netherlands

<sup>3</sup> The Maastricht Multimodal Molecular Imaging Institute, Maastricht University, Maastricht, The Netherlands

<sup>4</sup> Proteomics Center, Erasmus University Medical Center, Rotterdam, The Netherlands

<sup>5</sup> Single Cell Discoveries, Utrecht, The Netherlands

\*Corresponding author. Tel: +31 30 2121800; E-mail: h.clevers@hubrecht.eu

\*\*Corresponding author. Tel: +31 10 7044004; E-mail: b.haagmans@erasmusmc.nl

†These authors contributed equally to this work

‡These authors contributed equally to this work

detected by pattern recognition receptors (PRRs). PRR signaling subsequently leads to the transcription of antiviral genes; the response triggered varies between pulmonary cell types (preprint: Ravindra *et al*, 2020). Therefore, disease outcome can be greatly influenced by the viral target cell, which is determined largely by the presence of CoV entry receptor. In the lungs, angiotensin-converting enzyme 2 (ACE2), the SARS-CoV-2 receptor (Hoffmann *et al*, 2020; Walls *et al*, 2020; Wrapp *et al*, 2020; Zhou *et al*, 2020), is expressed mainly in ciliated cells and alveolar type II cells (Jia *et al*, 2005; Hikmet *et al*, 2020; Qi *et al*, 2020). Ciliated cells, alveolar type II cells, but also alveolar type I cells, have been identified as SARS-CoV-2 target cells in animal models and in COVID-19 patients (Hou *et al*, 2020; Rockx *et al*, 2020; Xu *et al*, 2020). In previous work, we confirmed ciliated cells as a viral target cell using organoid-derived bronchial airway cultures (Lamers *et al*, 2020). In contrast to ciliated cells, alveolar cells are notoriously difficult to culture, thus limiting our understanding of COVID-19, but also of other respiratory virus infections. Currently, standardized methods use immortal cell lines or primary alveolar cells to study disease (van den Bogaard *et al*, 2009). Immortal cell lines, however, do not fully recapitulate the complexity of the alveolar space and epithelium. Primary alveolar cells partially capture this complexity but remain incapable of undergoing passaging and quickly lose their *in vivo* phenotype which restricts the model by the availability of donor material (Logan & Desai, 2015; Zacharias *et al*, 2018). Importantly, primary adult alveolar cultures were recently shown to be poorly permissive to SARS-CoV-2 infection, emphasizing the urgent need to develop a susceptible SARS-CoV-2 alveolar infection model (Hou *et al*, 2020; Hui *et al*, 2020). Some induced pluripotent stem cell-derived models have been able to show alveolar differentiation (Gotoh *et al*, 2014; Dye *et al*, 2015; Jacob *et al*, 2017; Yamamoto *et al*, 2017; de Carvalho *et al*, 2019; van Riet *et al*, 2020), yet differentiation from primary lung cells has remained challenging.

Here, we describe a bronchioalveolar-like 2D air–liquid interface cell system by confocal and electron microscopy and mRNA expression analysis. In this model, alveolar cells, but also basal cells, and rare neuroendocrine cells, are grown from 3D self-renewing lung bud tip progenitor organoids. In this system, SARS-CoV-2 replication competence, tropism, and induced host responses were determined and compared to 2D differentiated small airway epithelium.

## Results

### Replication competence and tropism of SARS-CoV-2 in 2D differentiated small airway epithelium

Human bronchial airway epithelial (HAE) cell cultures are an established primary epithelial lung cell model to study respiratory virus infections. In these cultures, primary basal cells can be differentiated at air–liquid interface into mature airway cell types. It has already been shown that 3D self-renewing airway organoids can also be used as a source of basal cells in this culture system (Zhou *et al*, 2018; Sachs *et al*, 2019; Lamers *et al*, 2020). We first established this system using small airway basal cells (Appendix Fig S1A–C) and demonstrated that SARS-CoV-2 readily

infects human small airway organoid-derived epithelium cultured in 2D at air–liquid interface (ALI) (Fig 1). SARS-CoV-2 grew to relatively high titers on these cells, as shown by titration of VeroE6 cells (Fig 1A and B) and viral RNA quantification (Appendix Fig S1D). Shedding of virus occurred predominantly apically (Appendix Fig S1E and F). As we have previously shown for large airway (bronchial) cultures (Lamers *et al*, 2020), ciliated cells were extensively targeted by SARS-CoV-2 (Fig 1C). In addition, we noted rare infection of CC10<sup>+</sup> club cells (Fig 1D), but no infection of MUC5AC<sup>+</sup> goblet cells (Fig 1E).

### Establishment of a 2D differentiated bronchioalveolar-like model

Another 3D lung organoid system was developed by Nikolic *et al* (2017), but this system has not yet been applied in virology. In this system, culture conditions were established to support long-term self-renewal of multipotent SOX2<sup>+</sup>SOX9<sup>+</sup> lung bud tip progenitor cells which *in vivo* differentiate into both airway and alveolar cells. We grew these lung bud tip organoids (LBT) from canalicular stage human fetal lungs 16–17 pcw (post-conception weeks). In expansion medium, which activates EGF, FGF, and WNT signaling, and inhibits BMP and TGFβ, the vast majority of cells were SOX2<sup>+</sup>SOX9<sup>+</sup> (Fig 2A), but rare ATII-L were also detected in a subpopulation of organoids using the HTII-280 antibody which exclusively stains ATII cells in the human lung (Gonzalez *et al*, 2010) (Fig 2B). Organoid lines were maintained for > 14 passages without apparent change in morphology, or SOX2 and SOX9 expression. Next, we established a model that contains alveolar-like cells, which could be accessed from the apical side for infection experiments. We plated SOX2<sup>+</sup>SOX9<sup>+</sup> progenitor cells in Transwell inserts in differentiation medium. Based on recent literature, we reasoned that addition of human canalicular stage mesenchyme would provide cues for the survival of ATII-L cells and differentiation toward an alveolar fate (Barkauskas *et al*, 2013; Nikolic *et al*, 2017; Nikolic & Rawlins, 2017; Leeman *et al*, 2019). After reaching confluency, cells were differentiated for at least 14 days at ALI (Fig 2C). The addition of canalicular stage mesenchymal cells in the bottom compartment of the Transwell increased the frequency of HTII-280<sup>+</sup> cells (Appendix Fig S2A and B). After 14 days of differentiation at ALI, cultures consisted of both multilayered and single-layered squamous epithelium. The areas with a single layer of mostly thin epithelium contained cells expressing the ATI markers HOPX (Fig 2D) and HTI-56 (Fig 2E), as well as the mature ATII marker HTII-280 (Fig 2F) and LPCAT1 (Fig 2G) (Dobbs *et al*, 1999; Gonzalez *et al*, 2010; Gonzales *et al*, 2015). SFTPC<sup>+</sup> cells were present in the single-layered epithelium and the top layer of the multilayered areas (Fig 2H). The multilayered areas contained TP63<sup>+</sup> basal cells as a bottom layer (Fig 2I). Canalicular stage mesenchyme from different donors resulted in similar expression of alveolar markers (Fig EV1A–H), whereas some variation was observed in basal cell proliferation (Fig 1EVI and J). Using mass spectrometry on apical washes, we also detected secreted surfactant proteins SFTPA1, SFTPA2, SFTPB, and SFTPD (Appendix Fig S3). mRNA expression analysis of 3D LBT and confluent 2D cultures before (2D non-ALI) and after (2D ALI) exposure to air indicated that lung bud tip progenitor markers SOX9 and SOX2 were decreased during differentiation (Fig EV2A and B), while alveolar cell

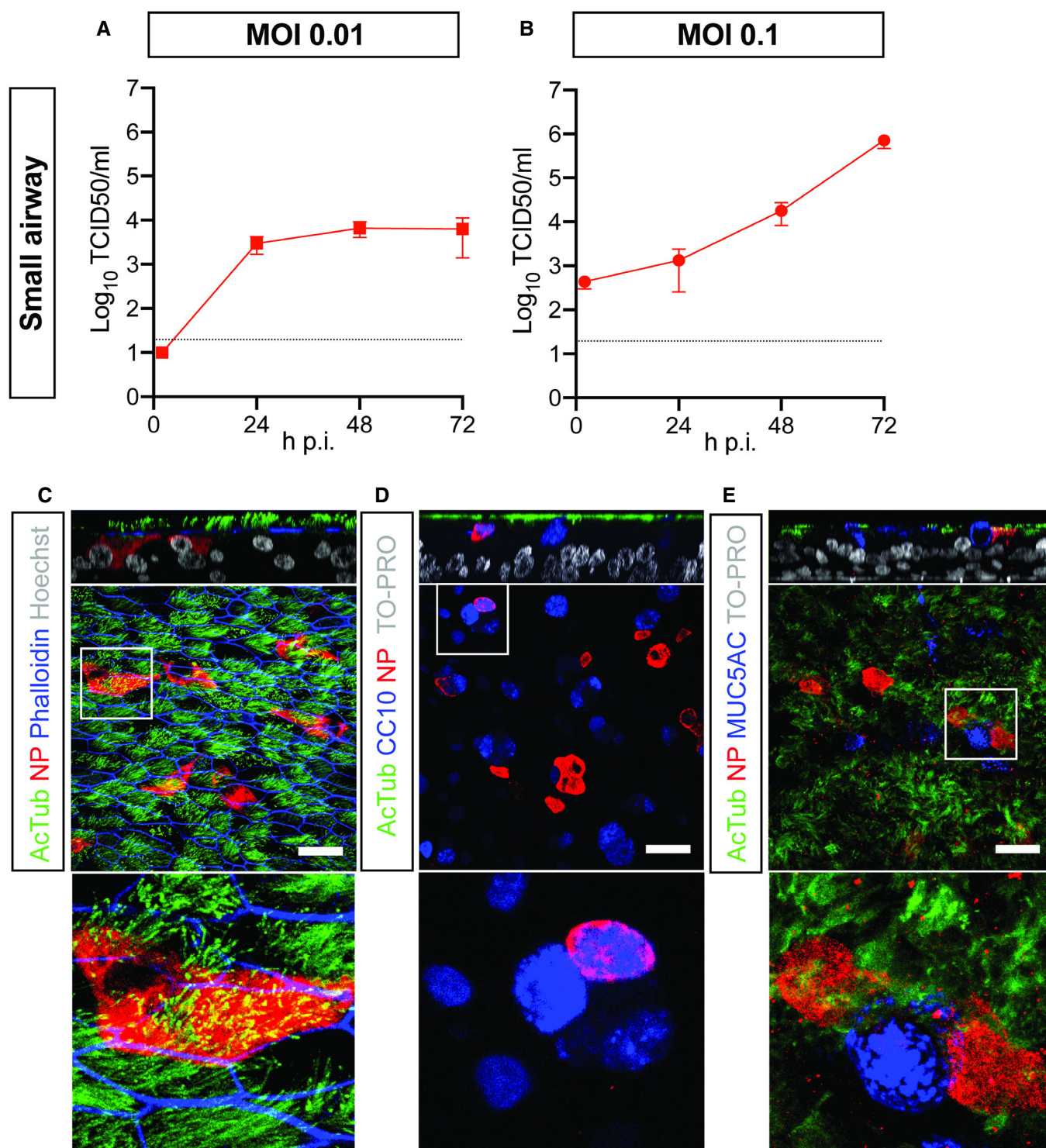


**Figure 1. SARS-CoV-2 infects human organoid-derived 2D small airway cultures.**

A, B Infectious virus titers can be observed by virus titrations on VeroE6 cells of apical washes at 2, 24, 48, and 72 h after infection at MOI 0.01 (A) or 0.1 (B) with SARS-CoV-2 (red). The dotted line indicates the lower limit of detection. Error bars represent SEM.  $N = 4$ . H p.i. = hours post-infection.

C–E Immunofluorescent staining of SARS-CoV-2 infected differentiated small airway cultures. Nucleoprotein (NP) stains viral capsid (red), which colocalized with the ciliated cell marker ActTUB (green; (C, D, E)) and club cell marker CC10 (blue; (D)). Phalloidin was included to stain actin (blue; (C)). Goblet cells are identified by MUC5AC (blue; (E)). Scale bars indicate 50  $\mu$ m.

Data information: Nuclei are stained with Hoechst or TOPRO and shown in white (C–E). Scale bars indicate 50  $\mu$ m.

markers SFTPA2, SFTPB, and HOPX gradually increased during differentiation (Fig EV2C–E). A general increase in ATI- and ATII-related genes from 3D LBT to 2D ALI cells was observed with intermediate levels at 2D non-ALI (Fig EV2F, Tables EV1 and EV2). The composition of cells in 2D ALI cultures was different from small airway ALI cultures, as indicated in differential expression analysis (Fig 3A, Table EV3). While small airway ALI cultures were mainly expressing ciliated cell markers like DNAH10 (Fig 3A), FOXJ1, and SNTN (Fig 3B), alveolar-like ALI cultures were enriched in ATI&II makers like HOPX and SFTPA1 (Fig 3). Moreover, 2D ALI cultures were enriched in markers for pulmonary neuroendocrine, tuft, and basal cells, while small airway cultures were enriched in goblet and ciliated cell markers (Fig 3B). All together, these data indicate that the 2D ALI cultures contain both alveolar-like and bronchiolar-like cells. These cultures could therefore be characterized as bronchioalveolar-like by confocal microscopy and mRNA expression analysis. The presence of pulmonary neuroendocrine cells (PNEC) was confirmed by confocal imaging (Appendix Fig S6B). The club and ATII cell marker SCGB3A2 was also detected in both single- and multilayered areas (Appendix Fig S6C).

To further investigate the diversity and frequency of the cell types in the bronchioalveolar system, we performed single-cell mRNA sequencing (Fig 4). This revealed a large alveolar-like cluster (94.3% of cells), a smaller basal cell cluster (4.9% of cells), and a rare population of PNECs (0.9% of cells) (Fig 4A). The alveolar cluster contained ATII-like cells (46.0% of cells, clusters 0 and 2) (Fig 4B–D; SFTPC, SFTPA1, LPCAT1; Appendix Fig S4A), proliferating ATII-like cells (6.4% of alveolar cells, cluster 4) (Fig 4E), and alveolar cells that showed an increased expression of several ATI markers (6.5% of alveolar-like cells, cluster 3) (Fig 4F–H; AGER, CAV1, HOPX; Appendix Fig S4B). The basal cell cluster (cluster 5) was characterized by KRT5 and TP63 expression (Fig 4I and J; Appendix Fig S4C). A rare PNEC population (cluster 7) expressed CHGA (Fig 4K; Appendix Fig S4D). To investigate whether the cultured cells were representative of adult alveolar cells, we compared our bulk RNA sequencing and single-cell RNA sequencing dataset to previously published bulk (Fig EV3A) and single-cell sequencing datasets (Figs 4L and M, and EV3B and C) of freshly isolated adult HTII-280<sup>+</sup> ATII cells. The freshly isolated adult ATII cells did not form a separate cluster in the t-SNE map (Fig 4L and M), and overlapped with cultured alveolar, proliferating alveolar and ATII-like cells (Figs 4M and EV3B). The expression of a set of ATII marker genes was also compared between the cultured ATII-like cluster and the freshly purified ATII cells (Fig EV3C). The SARS-CoV-2 entry receptor ACE2 was detected at low levels in the alveolar cluster (Fig 4N, Appendix Fig S5A), and ACE2 expression in ATII-like cells was confirmed by immunofluorescent imaging (Fig 4P). The activating protease TMPRSS2 was detected in all clusters with a higher expression in ATII-like cells (Fig 4O). In addition, there was a slight trend toward a correlation between ACE2 and TMPRSS2 expression (Appendix Fig S5A–D). At the protein level, both ACE2 and TMPRSS2 were readily detected and often coexpressed (Fig 4Q). Other TMPRSS-family members were detected in lower levels (Appendix Fig S5E–H). These data show that the bronchioalveolar model consists mainly of ATII-like cells and potentially is susceptible to SARS-CoV-2 infection.

### Replication competence and tropism of SARS-CoV-2 in 2D differentiated bronchioalveolar-like cultures

In order to also assess the replication competence and tropism of SARS-CoV-2 in bronchioalveolar-like cells, we infected these cultures with SARS-CoV-2. SARS-CoV-2 readily infected the cells at a low multiplicity of infection (MOI) of 0.01 and reached slightly higher titers at a MOI of 0.1, as shown by titration of VeroE6 cells (Fig 5A and B) and viral RNA quantification (Fig EV4A and B). Shedding of virus occurred predominantly apically (Fig EV4C and D). In these cultures, we observed infection of alveolar cells (Fig 5C–E) as evidenced by staining against HOPX, HTII-280, and SFTPC. Most infected cells appeared to be SFTPC<sup>+</sup> (Fig 5E). Using a marker for dividing cells (Ki67), we showed that infected cells were not dividing (Appendix Fig S6C). We did not detect infected PNEC in the top compartment, nor infected mesenchymal cells in the basal compartment.

### Transmission electron microscopy analysis of SARS-CoV-2 infected bronchioalveolar-like cells and small airway epithelial cells

Next, we performed transmission electron microscopy (TEM) to confirm SARS-CoV-2 infection inside the 2D bronchioalveolar-like (Fig EV4A–F) and 2D small airway (Fig EV5G–K) cultures at high magnification. Upon inspection of the 2D bronchioalveolar-like culture, ATII-L were readily classified (Fig EV5A and B) based on the presence of lamellar bodies (Fig EV5D). SARS-CoV-2 infection was found in ATII-L cells (Fig EV5C and D) and showed early infection onset with few double membrane vesicles and both electron dense (Fig EV5D) and lucent (Fig EV5C) compartments harboring virus particles. Interestingly, next to the ATII-L cell, a fragmented dead cell is visible (Fig EV5F) with many extracellular virus particles still attached to the apical side and only few particles present on the basal side. This suggests that virus shedding mainly occurs on the air-faced side inside lung tissue. Nonetheless, also in between the ATII-L cells and an adjacent cell, some virus particles were detected, although it is not clear whether these sites are also the place of virion secretion or whether virions can diffuse between the cell layers. The latter is implausible due to the lack of detectable infectious virus in the basal compartment of the culture. Similarly, also the 2D small airway cultures (Fig EV5G–K) were examined with TEM and contained a confluent layer consisting mainly of ciliated cells (Fig EV5H–J) along with club cells and goblet cells (Fig EV5K). In accordance with confocal microscopy findings, at 72 h post-infection, morphological evidence of SARS-CoV-2 infection, replication, and assembly was found inside ciliated cells (Fig EV5I). Secreted virions were again found at the apical side next to the still intact cilia (Fig EV5J), whereas no viruses were found at the basal side. Using confocal microscopy, we also detected rare infection of club cells (Fig 1D), but these rare events could not be visualized by TEM thus far.

### Host responses induced by SARS-CoV-2 in bronchioalveolar-like cells and small airway epithelial cells

To investigate the cellular response to infection, we stained bronchioalveolar-like and small airway cultures for phosphorylated



STAT1 (pSTAT1) at 72 h post-infection. STAT1 is phosphorylated in response to interferon (IFN) receptor signaling, which promotes translocation of STAT1 to the nucleus where it stimulates the expression of interferon-stimulated genes (ISGs). We observed STAT1 phosphorylation and nuclear translocation in bystander cells

of SARS-CoV-2 infected cultures in both bronchioalveolar-like (Fig 6A) and small airway (Fig 6C) cultures, but not in infected cells, indicating potentially active blocking of the JAK/STAT pathway in infected cells. Active blocking of STAT1 nuclear import has been reported for SARS-CoV. SARS-CoV ORF6 antagonizes STAT1

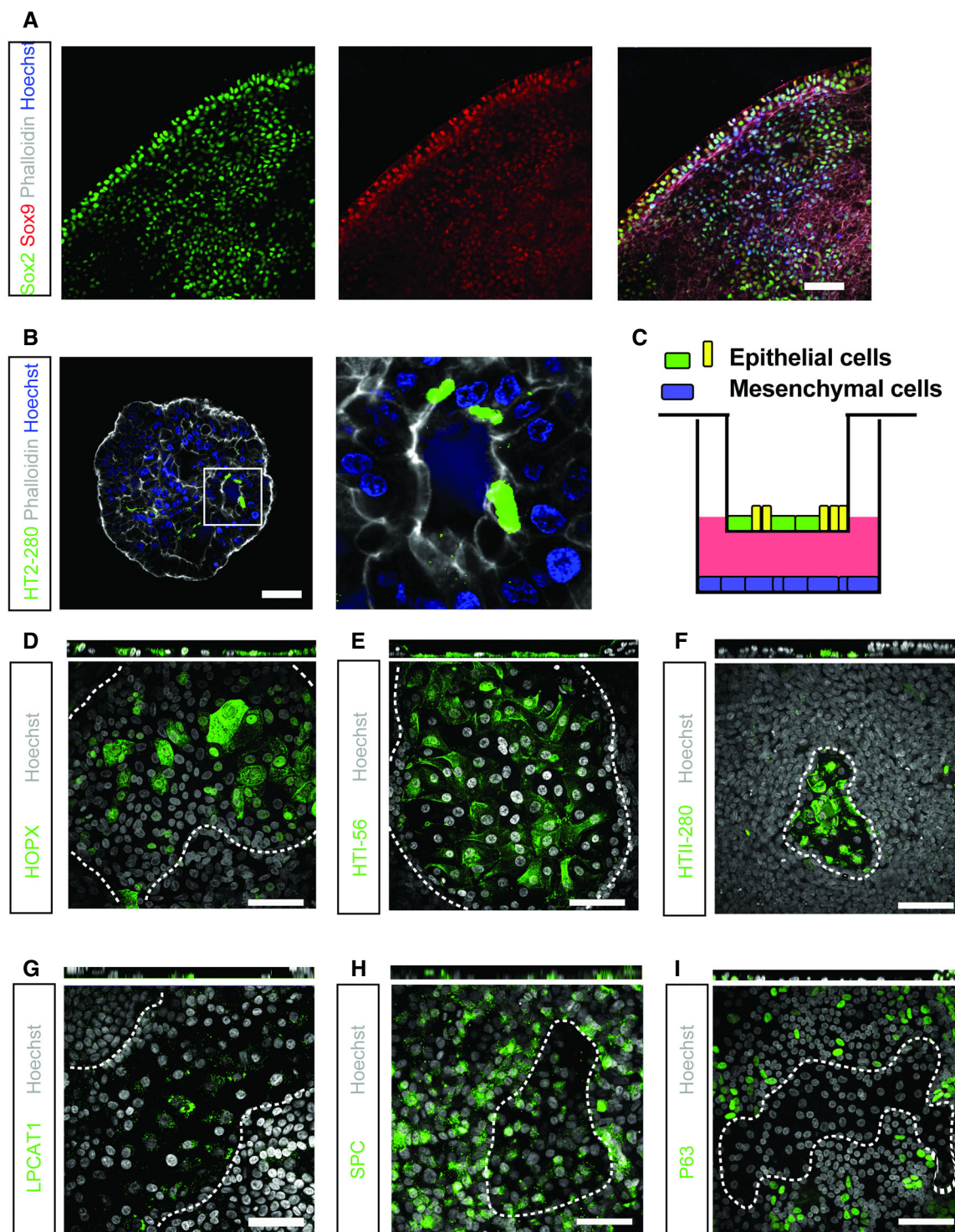
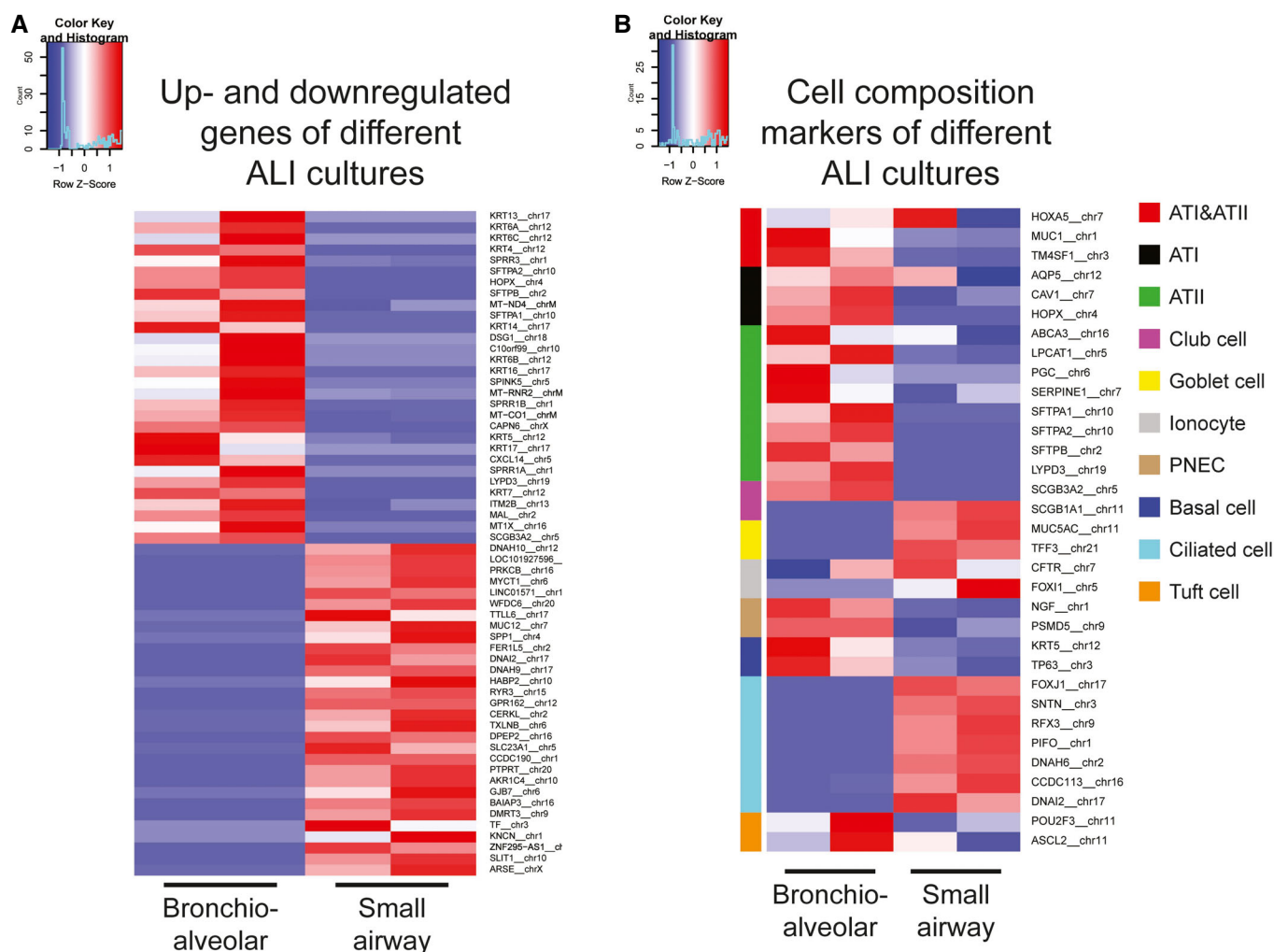


Figure 2.

**Figure 2. Self-renewing human fetal lung bud tip progenitor organoids differentiate at air–liquid interface to alveolar type I- and type II-like cells.**

- A Immunofluorescent staining of fetal lung bud tip progenitor organoids grown in expansion medium co-expressing stem cell markers Sox2 (green) and Sox9 (red). Phalloidin (white) was used to stain actin.
- B Immunofluorescent staining of rare HTII-280 + type II pneumocytes (green) in a subpopulation of fetal lung bud tip progenitor organoids grown in expansion medium.
- C Schematic of the 2D air–liquid interface bronchioalveolar-like model.
- D–I Differentiated lung bud tip organoids at air–liquid interface in co-culture with donor-specific human fetal lung fibroblasts. After 14 days of differentiation at air–liquid interface, cells express alveolar type I (HOPX, green, (D)); HTI-56, green, (E)), type II cells (HTII-280, green, (F); LPCAT1, green, (G); SFTPC (SPC), green, (H)), and basal cell (TP63 (P63), green, (I)) markers in areas containing one cell layer. Dotted lines indicate the barrier between multilayered and single-layered epithelium.

Data information: Nuclei are stained with Hoechst (blue in (A, B) or white in (D–I)). Scale bars indicate 50  $\mu$ m.

**Figure 3. Transcriptomic analysis of bronchioalveolar-like and small airway air–liquid interface cultures.**

- A Heatmaps depicting top 30 up- and downregulated genes in 2D bronchioalveolar-like air–liquid cultures (bronchioalveolar) compared to small airway air–liquid interface cultures (small airway). Colored bars represent Z-scores of  $\log_2$ -transformed values.
- B Heatmaps depicting pulmonary cell type marker genes in 2D bronchioalveolar-like air–liquid cultures (bronchioalveolar) and small airway air–liquid interface cultures (small airway). Color-coded bars indicate which cell type is marked by the presented gene. Colored bars represent Z-scores of  $\log_2$ -transformed values.

function by sequestering nuclear import factors on the rough endoplasmic reticulum/Golgi membrane (Frieman *et al*, 2007; Kopecky-Bromberg *et al*, 2007). Whether SARS-CoV-2 ORF6 has similar

functions remains to be investigated, but recently the SARS-CoV-2 N protein was shown to suppress the translocation of STAT1 and STAT2 (Mu *et al*, 2020).

Next, we performed mRNA sequencing analysis to determine gene expression changes induced by SARS-CoV-2-infection of bronchioalveolar-like cultures. As suggested by pSTAT1 translocation, infection with SARS-CoV-2 elicited a broad signature of interferon-stimulated genes (ISGs) attributed to type I/III interferon responses (Fig 6B and D), which was confirmed by Gene Ontology analysis (Fig 6E and F) in both bronchioalveolar-like

(Fig 6B and E, Table EV4) and small airway cultures (Fig 6D and F, Table EV5). This induction was similar to earlier reported SARS-CoV-2 infection in human bronchial epithelial cells (Blanco-Melo *et al*, 2020) and indicated induction of strong chemotactic and inflammatory responses. Generally, the responses to SARS-CoV-2 appeared similar between the two pulmonary systems.

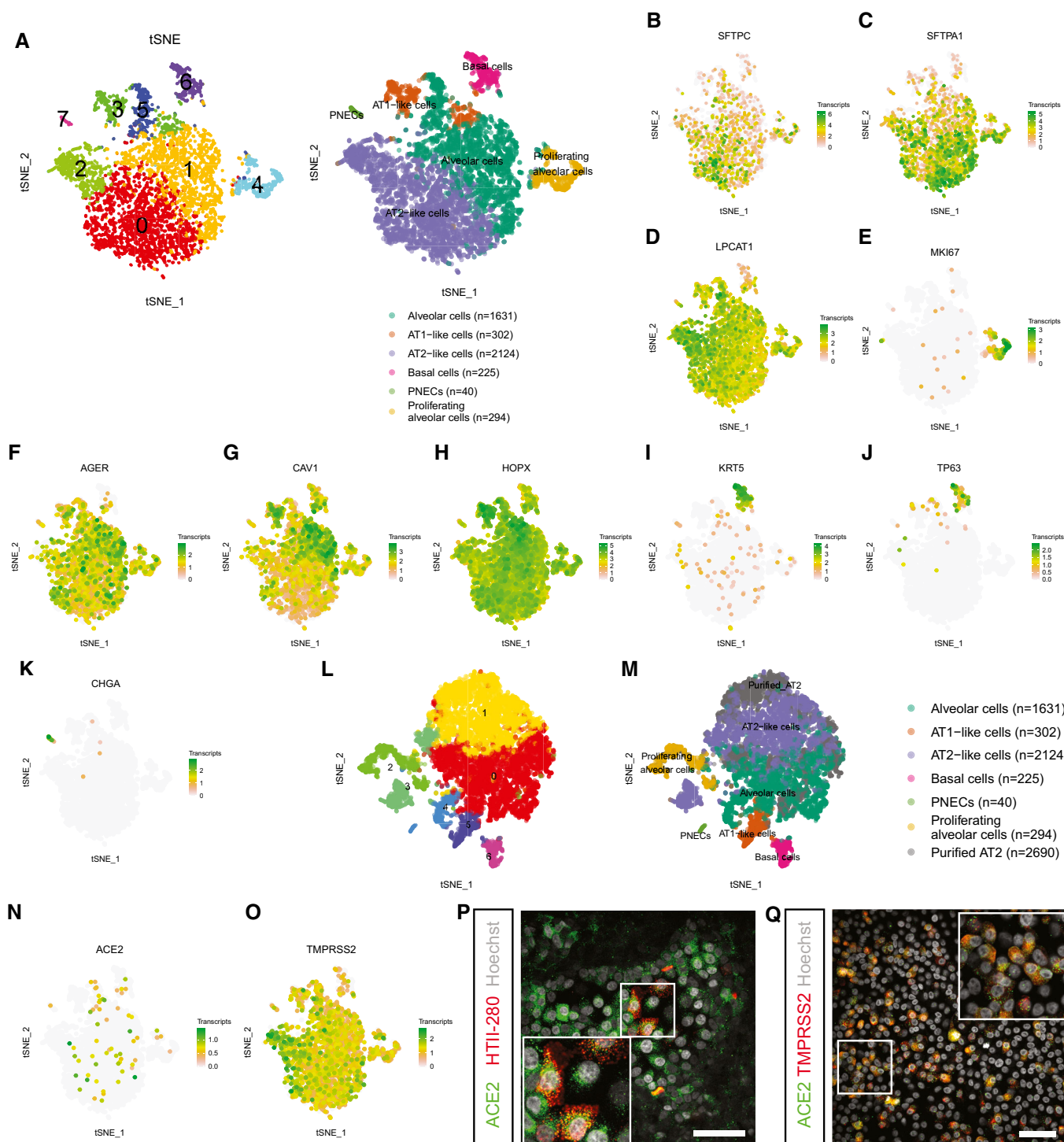


Figure 4.



**Figure 4. Single-cell analysis of bronchioalveolar cultures.**

- A t-SNE maps showing clustering based on differentially expression analysis and highlighting cell type identification of bronchioalveolar cultures based on cell makers. Each color represents a cluster or different cell type. Number indicates number of cells in cluster identified as cell type presented.
- B–K t-SNE maps highlighting the expression of marker genes for each of the cell types. Transcript counts are given in a Log<sub>2</sub> scale.
- L t-SNE map showing clustering based on differentially expression analysis including dataset from (A) and published dataset of GSM2855485. Each color represents a single cluster.
- M t-SNE map showing clustering of (L) with annotation of cell types. Cell type annotation is transferred from (A), and published dataset GSM2855485 is annotated as “Purified AT2”. Number indicates number of cells in cluster identified as cell type presented.
- N, O t-SNE maps highlighting the expression of SARS-CoV-2 entry receptors ACE2 (N) and TMPRSS2 (O). Transcript counts are given in a Log<sub>2</sub> scale.
- P Differentiated bronchioalveolar cultures express SARS-CoV-2 entry receptor ACE2 (green) on ATII-like cells marked by HTII-280 (red). Nuclei are stained with Hoechst and shown in white. Scale bar indicates 50 μm.
- Q Bronchioalveolar cultures co-express both entry receptors ACE2 (green) and TMPRSS2 (red). Nuclei are stained with Hoechst and shown in white. Scale bar indicates 50 μm.

To test the suitability of the bronchioalveolar model for SARS-CoV-2 drug screens, we analyzed the effect of IFN-λ1 on viral replication. For this experiment, cultures were treated with IFN-λ1 (50 ng/ml) 2 h prior to infection at an MOI of 0.1 or 24 h after infection. In the untreated control, SARS-CoV-2 replicated to high titers, approaching 10<sup>6</sup> TCID<sub>50</sub> or 10<sup>8</sup> viral copies per ml (Fig 7A and B). Pre-treatment with IFN-λ1 abrogated viral replication entirely and treatment at 24 h post-infection reduced infectious virus and RNA copies by ~ 5 logs and ~ 3 logs, respectively. These differences were also apparent by confocal imaging at 72 h post-infection (Fig 7C). This bronchioalveolar culture system can therefore be applied to test COVID-19 therapeutics.

## Discussion

In COVID-19 patients, alveolar injury can trigger a cascade of events that leads to ARDS, limiting the transport of oxygen into the blood. A plethora of models are currently being developed to study this. *In vivo* models can be very useful, but are often extremely difficult and expensive to establish and may not represent conditions in humans. Most *in vitro* models utilize cell lines or primary cells that are often limited by the availability of donor materials and show donor–donor variation. In addition, primary human alveolar cultures are poorly susceptible to SARS-CoV-2 infection (Hou *et al*, 2020; Hui *et al*, 2020). Self-renewing organoid models that contain stem cells which can differentiate into relevant cell types offer an elegant solution to develop human models that can be standardized. While a robust self-renewing organoid model exists for the airway epithelium, the alveolar epithelium has proven very difficult to establish. As the alveolar epithelium is thought to play a major role in the disease progression of COVID-19, the lack of an *in vitro* model greatly limits our understanding of this disease, but also of other respiratory virus infections.

This study shows that SARS-CoV-2 efficiently replicates in a human bronchioalveolar-like model, targeting ATII-L cells. This study is in accordance with clinical findings that SARS-CoV-2 infects alveolar cells in COVID-19 patients. However, the variable incidence and severity of lower lung disease, and recent findings that alveolar cells have low levels of ACE2 expression in health, indicates that alveolar cells are unlikely to be the first cells infected through microaerosol inhalation of virus particles (Hou *et al*, 2020). Ciliated cells in the airways seem to express ACE2 more constitutively, with increasing expression toward the

proximal part of the airway (Hikmet *et al*, 2020; Hou *et al*, 2020). Using an organoid-derived small airway model, we show that ciliated cells are indeed the main target cell in the small airways, as was observed recently for primary small airway cells (Hou *et al*, 2020). Therefore, ciliated cells could be infected prior to the alveoli, with inflammatory or antiviral signals possibly leading to increased ACE2 expression as this gene was recently shown to be induced by interferon (Ziegler *et al*, 2020). Treatment of the bronchioalveolar cultures with a low dose of interferon lambda 1 was highly effective in reducing viral replication and dissemination, underscoring the high interferon sensitivity of this virus and indicating that interferons are a viable treatment option. Organoid-derived alveolar-like and airway models are ideal models to study these aspects of COVID-19.

This model has several limitations. In human fetal development, alveolar cells are derived from bipotent progenitor cells, whereas in adults, ATI cells are derived from a rare self-renewing population of ATII cells (Barkauskas *et al*, 2013; Nikolic *et al*, 2017). In adult mice, an additional cell type, the bronchioalveolar stem cell (BASC) (Kim *et al*, 2005), differentiates into both bronchiolar and alveolar cells, but in adult humans, such bipotent progenitors have not been identified yet. Fetal and adult alveolar cells may therefore be phenotypically distinct and may respond differentially to infections. In addition, mesenchymal cells improved alveolar development in 2D and future work should focus on identifying which mesenchymal cues drive this. On the other hand, the presence of mesenchymal cells could offer an interesting opportunity to study differential expression of genes involved in lung fibrosis as well in these cells.

This model also has several advantages. The bronchioalveolar-like model presented here shows a robust increase in infectious virus titers over time of ~ 5 logs, whereas other recently developed adult-derived 3D alveolar organoid models show a more limited increase in viral titers (~ 1–2 logs) (Katsura *et al*, 2020; Salahudeen *et al*, 2020; Youk *et al*, 2020). This allows for a larger window to observe antiviral effects of potential drugs. In addition, in our model, pulmonary epithelial cells are infected from and shed virus apically, while in most 3D organoid models, the apical side of the cells is facing the inside of the organoid. In the bronchioalveolar-like model presented here, the apical side of the cells is exposed to the air, which makes it is easily accessible, physiologically relevant and highly suitable for (high-throughput) virology studies. Similar results may be obtained with the recently developed iPSC-derived 2D ATII-like cultures (Huang *et al*, 2020). In addition, the modular



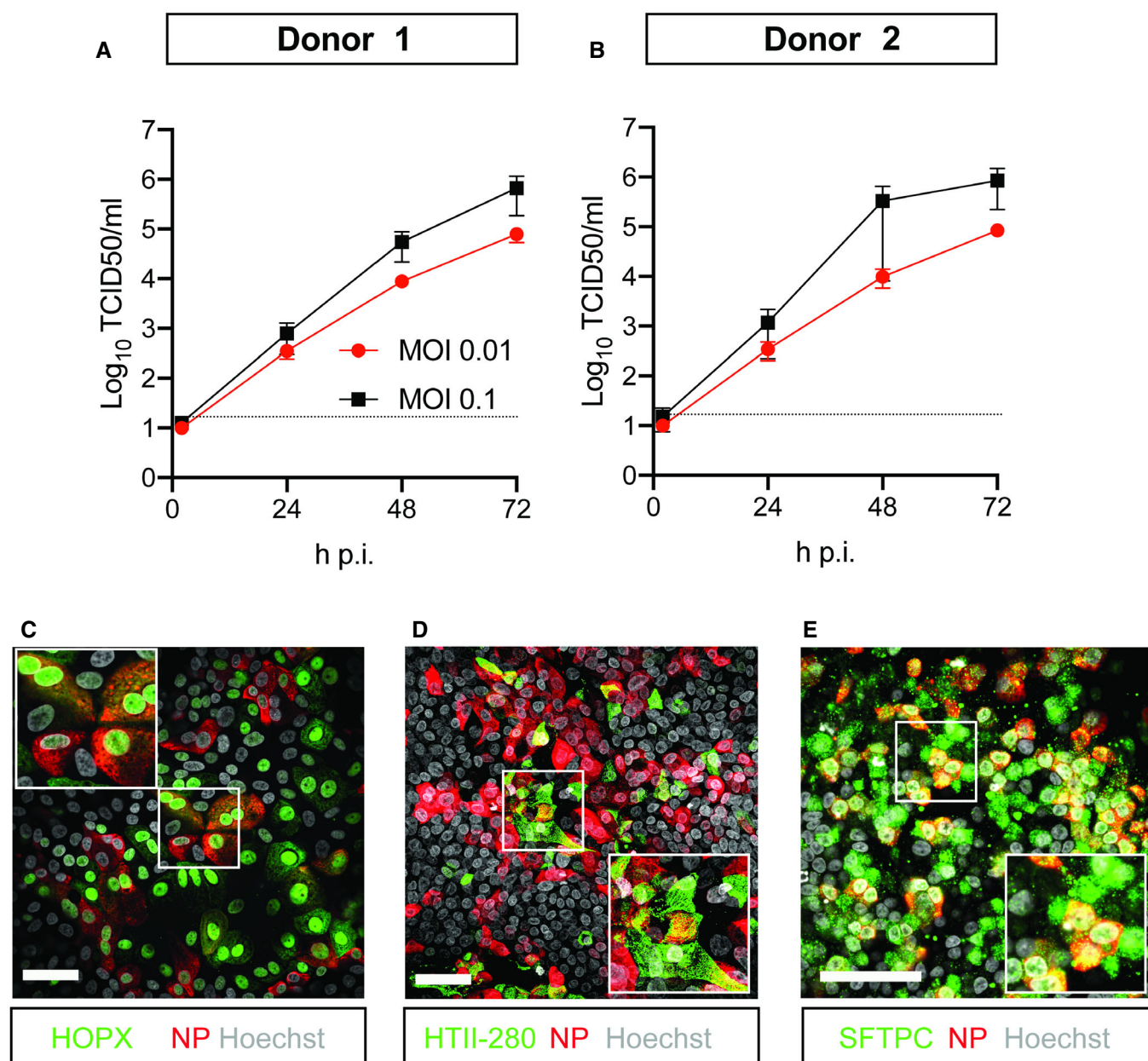


**Figure 5. SARS-CoV-2 infects human organoid-derived 2D bronchioalveolar-like cultures.**

A, B Infectious virus titers can be observed by virus titrations on VeroE6 cells of apical washes at 2, 24, 48, and 72 h after infection of bronchioalveolar-like cells from donor 1 (A) and donor 2 (B) at MOI 0.01 (red) or 0.1 (black) with SARS-CoV-2. The dotted line indicates the lower limit of detection. Error bars represent SEM.  $N = 4$  for all except donor 2 MOI 0.1, which is  $N = 3$ . H p.i. = hours post-infection.

C–E Immunofluorescent staining of SARS-CoV-2-infected differentiated bronchioalveolar-like cultures. Nucleoprotein (NP) stains viral capsid (red), which colocalized with HOPX (C), HTII-280 (D), and SFTPC (E). Scale bars indicate 50  $\mu$ m. Nuclei are stained with Hoechst and shown in white (C–E).

Transwell setup allows the addition of other cell types. For example, endothelial cells would be of interest, as the lungs of deceased COVID-19 patients were recently found to show distinctive vascular features, including endothelialitis, widespread thrombosis with microangiopathy, and angiogenesis (Ackermann *et al*, 2020). In addition, immune cells could be added, which may be relevant as severe COVID-19 symptoms and hospitalization often occur ~8–15 days after disease onset (Lauer *et al*, 2020) indicating that acute

lung injury may be the result of an overreaction of the immune system, rather than a direct effect of virus replication. As this model is derived from self-renewing organoids, it is also amenable to genetic manipulation using CRISPR/Cas systems, which allows the study of specific host factors. Intrinsically, the model is also suitable for pulmonary cell and developmental biology studies, especially for studies on the interaction between epithelial and mesenchymal cells without the need for physical interaction.

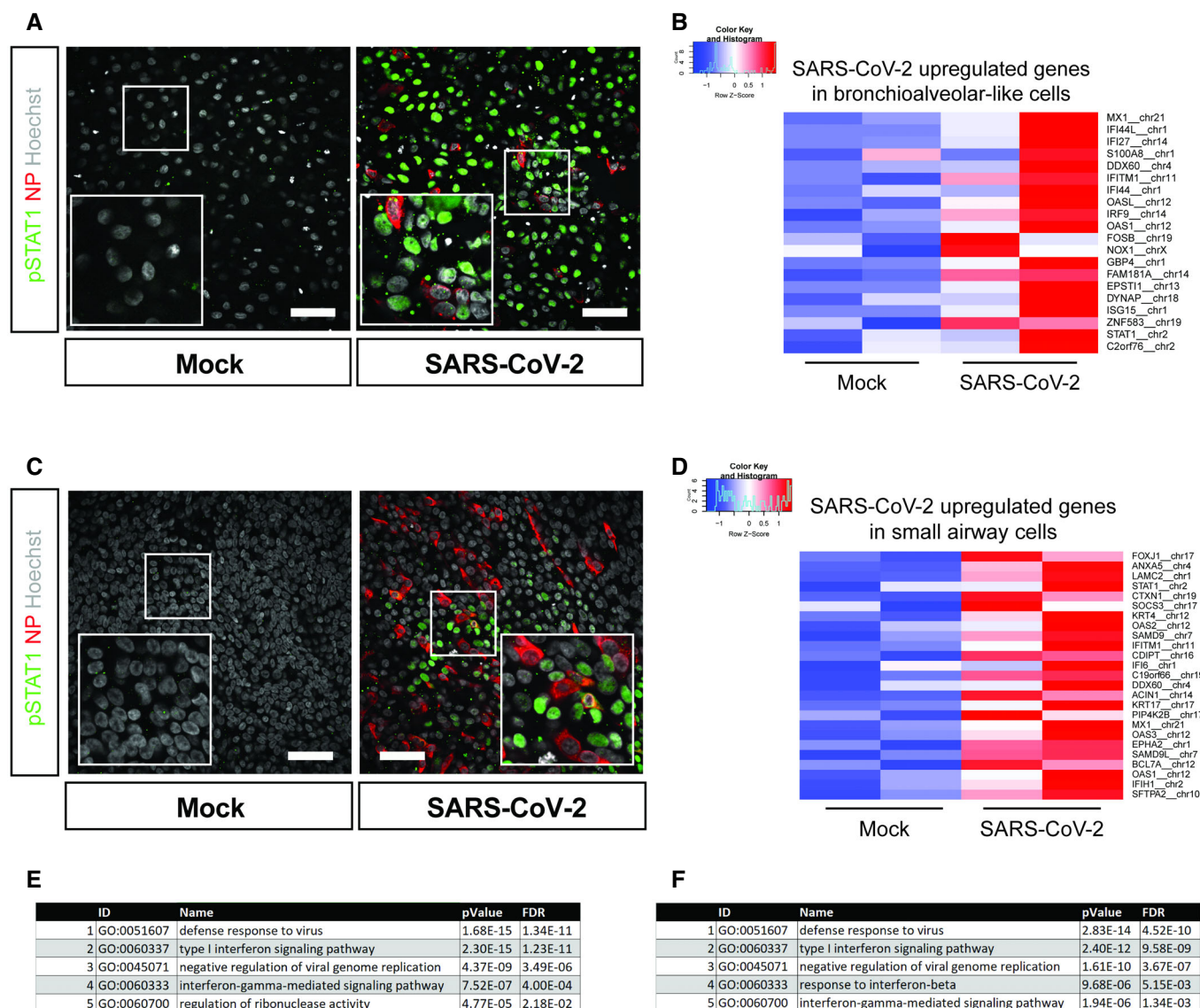


**Figure 6. Host response analysis of SARS-CoV-2 infection in organoid-derived bronchioalveolar-like and small airway cells.**

- A pSTAT1 translocation in mock and SARS-CoV-2-infected bronchioalveolar-like cells visualized in green. Scale bars indicate 50  $\mu$ m. Nucleoprotein (NP) stains viral capsid (red). Nuclei are stained with Hoechst (white). Scale bar indicates 50  $\mu$ m.
- B Heatmaps depicting top 20 enriched genes based on adjusted *P*-value in bronchioalveolar-like cells after SARS-CoV-2 infection. Colored bars represent Z-scores of log<sub>2</sub>-transformed values.
- C pSTAT1 translocation in mock and SARS-CoV-2-infected small airway cells visualized in green. Nucleoprotein (NP) stains viral capsid (red). Nuclei are stained with Hoechst (white). Scale bar indicates 50  $\mu$ m.
- D Heatmaps depicting top 25 enriched genes based on adjusted *P*-value and log<sub>2</sub> fold changes in small airway cells after SARS-CoV-2 infection. Colored bars represent Z-scores of log<sub>2</sub>-transformed values.
- E GO term enrichment analysis for biological processes of the 20 most significantly up-regulated genes upon SARS-CoV-2 infected in bronchioalveolar-like cells. *P*-values were determined using PANTHER Overrepresentation Test.
- F GO term enrichment analysis for biological processes of the 25 most significantly up-regulated genes upon SARS-CoV-2 infected in small airway cells. *P*-values were determined using PANTHER Overrepresentation Test.

In conclusion, bronchioalveolar-like cells derived from self-renewing human fetal lung organoids give rise to a 2D human bronchioalveolar-like model with air-exposed apical side. In these cultures, alveolar type II-like cells are permissive to SARS-CoV-2

infection, which induces a type I/III interferon host response *in vitro*. SARS-CoV-2 replication is abrogated by low-dose interferon lambda 1 treatment, showing that this model system can be used for COVID-19 drug screens.

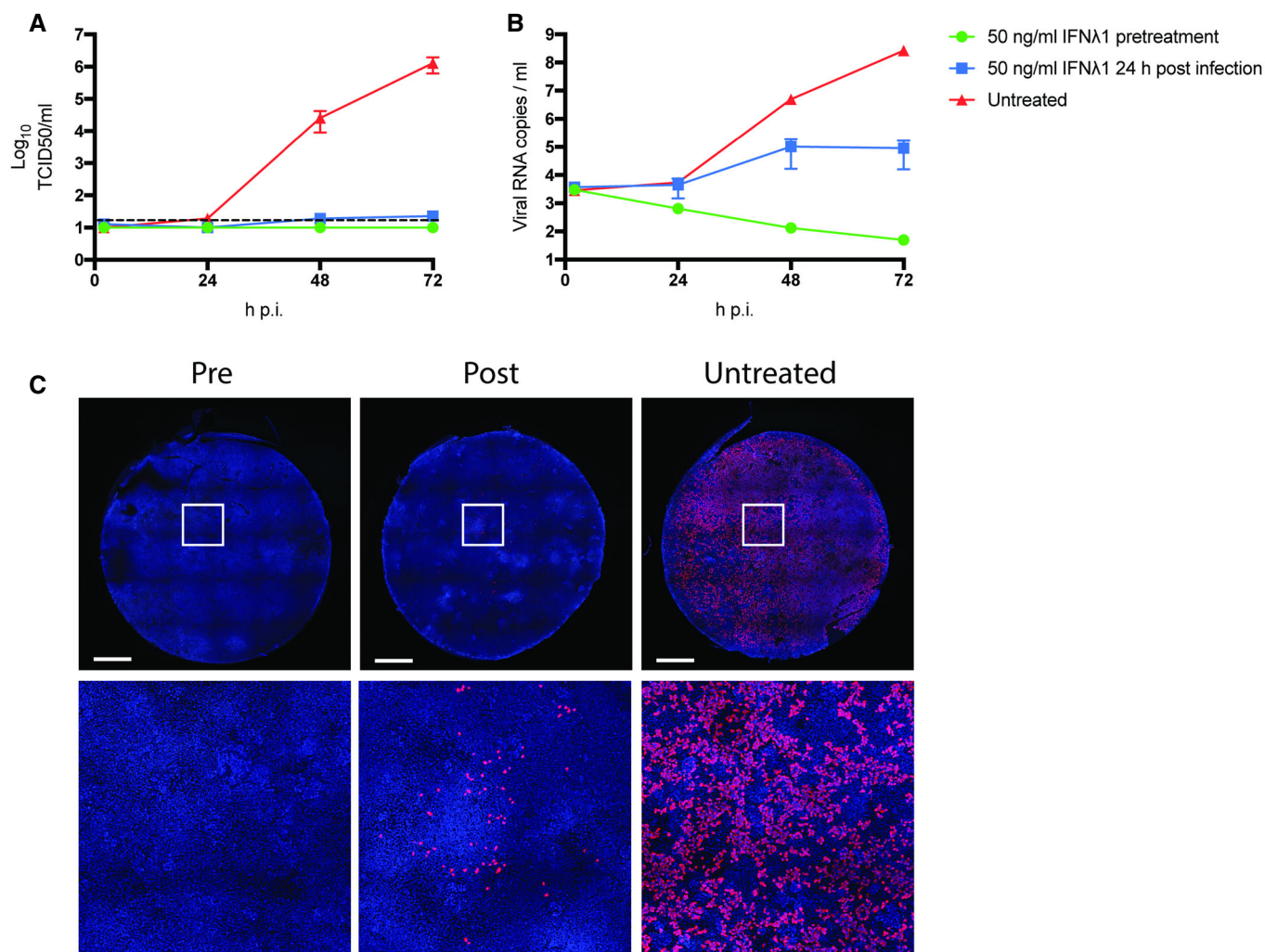


**Figure 7. Low-dose interferon lambda 1 treatment dramatically reduces SARS-CoV-2 replication in bronchioalveolar-like cultures.**

**A, B** SARS-CoV-2 replication shown as infectious virus titers (**A**) and viral RNA copies (**B**) in apical washes at 2, 24, 48, and 72 h after infection at MOI 0.1. Cultures were either pretreated with 50 ng/ml IFN lambda 1 in the basal compartment 2 h prior to the infection (green), at 24 h p.i. or left untreated. The dotted line indicates the lower limit of detection. Error bars represent SEM. *N* = 2. H p.i. = hours post-infection.

**C** Whole well immunofluorescent staining of representative cultures in (**A**) and (**B**) using an anti-NP antibody (red). Nuclei are stained with Hoechst (blue). Scale bar indicates 1 mm.

Materials and Methods

Reagents and Tools table

Reagent/Resource	Reference or Source	Identifier or Catalog Number
Experimental Models		
SARS-CoV-2 BavPat1	C. Drosten	European Virus Archive Global #026V-03883
Small airway organoids	This study	
Lung bud tip organoids Donor 1 (#19162)	This study	
Lung bud tip organoids Donor 2 (#2)	This study	
VeroE6 cells	ATCC	CRL 1586TM
Recombinant DNA		
N/A		

Reagents and Tools table (continued)

Reagent/Resource	Reference or Source	Identifier or Catalog Number
<b>Antibodies</b>		
Mouse-anti-SARS-CoV NP (monoclonal)	Sino Biological	40143-MM05
Rabbit-anti-SARS-CoV NP (polyclonal)	Sino Biological	40143-T62
Mouse-anti-HTII-280 (monoclonal)	Terrace Biotech	TB-27AHT2-280
Rabbit-anti-SFTPC (polyclonal)	Santa Cruz	FL-197
Rabbit-anti-HOPX (polyclonal)	Santa Cruz	sc-30216
Mouse-anti-HTI-56 (monoclonal)	Terrace Biotech	TB-29 AHTI-56
Mouse-anti-MUC5AC (monoclonal)	Invitrogen	MA5-12178
Anti-LPCAT1 (polyclonal)	Sigma	HPA012501
Mouse-anti-CC10 (monoclonal)	Santa Cruz	sc-390313 AF594
Goat-anti-SCGB3A2 (polyclonal)	R&D systems	AF3545
Mouse-anti-ActUB (monoclonal)	Santa Cruz	sc-23950 AF488
Rabbit-anti-pSTAT1 (monoclonal)	Thermo Fisher	MA5-15071
Mous-anti-Ki67 (monoclonal)	DAKO	GAG2661-2
Mouse-anti-ZO-1 (monoclonal)	Invitrogen	ZO1-1A12
Mouse-anti-SOX2 (monoclonal)	Santa Cruz	sc-365823 AF488
Mouse-anti-SOX9 (monoclonal)	Santa Cruz	sc-166505 AF594
Mouse-anti-TP63 (monoclonal)	Abcam	ab735
Mouse-anti-SYP	Santa Cruz	sc-17750
Rabbit-anti-ACE2	Atlas antibodies	HPA000288
Mouse-anti-TMPRSS2	Santa Cruz	sc-515727
Goat-anti-mouse IgM 594	Invitrogen	A21044
Goat-anti-mouse IgG 488	Invitrogen	A11029
Goat-anti-mouse IgG2a 488	Invitrogen	A21131
Goat-anti-rabbit IgG 488	Invitrogen	A32731
Rabbit-anti-goat IgG 594	Invitrogen	A11080
Rabbit-anti-goat IgG 488	Invitrogen	A11078
Goat-anti-mouse IgG1 594	Invitrogen	A21125
Goat-anti-rabbit IgG 594	Invitrogen	A11012
Goat-anti-mouse IgM 488	Invitrogen	A21042
<b>Oligonucleotides and other sequence-based reagents</b>		
SARS-CoV-2 E gene taqman	Corman <i>et al</i> (2020)	
CEL-seq2-based SORT-seq primers	Hashimshony <i>et al</i> (2016), van den Brink <i>et al</i> (2017)	
Illumina Truseq small RNA primers	Illumina	
10x genomics primers and reagents V3.1	10× Genomics	
<b>Chemicals, enzymes and other reagents</b>		
Advanced DMEM/F12	Gibco	12634010
Glutamax	Gibco	35050061
AO medium	Sachs <i>et al</i> (2019)	
FL medium	Nikolic <i>et al</i> (2017)	
Opti-MEM I (1×) + GlutaMAX	Gibco	51985-042
HEPES	Lonza	BE17-737E
Penicillin-Streptomycin Mixture (Pen/Strep)	Lonza	DE17-602E
Hoechst	Thermo Fisher	H1399
DAPI	Sigma	D9542



**Reagents and Tools table** (continued)

Reagent/Resource	Reference or Source	Identifier or Catalog Number
TO-PRO-3	Thermo Fisher	T3605
Phalloidin	Santa Cruz	ec-363796
Prolong Diamond Antifade	Invitrogen	P36961
red blood cell lysis buffer	Roche	11814389001
Matrigel (GFR)	Corning	#356231
Dispase	Corning	#354235
TrypLE express	Gibco	12604-013
Stemcell Pneumacult-ALI	Stemcell	#05001
Hibernate A	Gibco	#A1247501
BEpiCM	Sciencell	#3211
Basal medium	Sciencell	#3211-b
BEpiCGS	Sciencell	#3262
Retinoic acid	Sigma	R2625
ROCK inhibitor	Sigma	Y0503
MagnaPure LC Lysis buffer	Roche	05323738001
Agencourt AMPure XP beads	Beckman Coulter	A63882
MagnaPure LC elution buffer	Roche	05323738001
TaqMan™ Fast Virus 1-Step Master Mix	Applied Biosystems	4444436
Laemmli buffer	Bio Rad	#161-0747
Dithiothreitol	Sigma	D8255
iodoacetamide	Sigma	I6125
Sera-Mag SpeedBeads	Fisher Scientific	09-981-123
TRIzol	Thermo Fisher	15596026
Pepmap C18 column	Thermo Fisher	164564
IFN-L1	Peprtech	300-02L
<b>Software</b>		
ZEN software	ZEISS	
Prism 8	Graphpad	
Cell Ranger 4.0.0	10× Genomics	
Rstudio v 1.1.463	Rstudio	
Seurat v 3	Satija lab, NYU Genome Centre	
<b>Other</b>		
DynaMag-96	Invitrogen	12331D
LSM700	Zeiss	
Transwell inserts	Corning	3260 & 3270
Orbitrap Eclipse Tribrid mass spectrometer	Thermo Fisher	
Illumina Nextseq500	Illumina	
Tecnai T12 microscope	FEI	
10× Genomics chromium controller	10× Genomics	

## Methods and Protocols

### Viruses and cells

Vero E6 cells were maintained in Dulbecco's modified Eagle's medium (DMEM, Gibco) supplemented with 10% fetal calf serum (FCS), HEPES, sodium bicarbonate, penicillin (100 IU/ml), and

streptomycin (100 IU/ml) at 37°C in a humidified CO<sub>2</sub> incubator. SARS-CoV-2 (isolate BetaCoV/Munich/BavPat1/2020; European Virus Archive Global #026V-03883; kindly provided by Dr. C. Drosten) was propagated on VeroE6 (ATCC® CRL 1586TM) cells in Opti-MEM I (1×) + GlutaMAX (Gibco), supplemented with penicillin (100 IU/ml) and streptomycin (100 IU/ml) at 37°C in a humidified

CO<sub>2</sub> incubator. The SARS-CoV-2 isolate was obtained from a clinical case in Germany, diagnosed after returning from China. Stocks were produced by infecting VeroE6 cells at a multiplicity of infection (MOI) of 0.01 and incubating the cells for 72 h. The culture supernatant was cleared by centrifugation and stored in aliquots at  $-80^{\circ}\text{C}$ . Stock titers were determined by preparing 10-fold serial dilutions in Opti-MEM 1 (1 $\times$ ) + GlutaMAX. Aliquots of each dilution were added to monolayers of  $2 \times 10^4$  Vero E6 cells in the same medium in a 96-well plate. Twenty-four replicates were performed per virus stock. Plates were incubated at  $37^{\circ}\text{C}$  for 5 days and then examined for cytopathic effect. The TCID<sub>50</sub> was calculated according to the method of Spearman & Kärber. All work with infectious SARS-CoV and SARS-CoV-2 was performed in a Class II Biosafety Cabinet under BSL-3 conditions at Erasmus Medical Center.

### SARS-CoV-2 infection

2D differentiated cultures were washed twice with 200  $\mu\text{l}$  Advanced DMEM/F12 (Gibco) with Glutamax (Gibco), HEPES (Lonza), penicillin (100 IU/ml), and streptomycin (100 IU/ml) (Lonza) (AdDF+++), before inoculation from the apical side at a MOI of 0.01 or 0.1 (as indicated) in 200  $\mu\text{l}$  AdDF+++ per well. The number of cells in each culture was calculated by trypsinizing and counting the cells from 1 well. Next, cultures were incubated at  $37^{\circ}\text{C}$  5% CO<sub>2</sub> for 2 h before washing three times in 200  $\mu\text{l}$  AdDF++. At the indicated timepoints, virus was collected from the cells by adding 200  $\mu\text{l}$  AdDF+++ apically, incubating 10 min at  $37^{\circ}\text{C}$  5% CO<sub>2</sub>, and storing the supernatant at  $-80^{\circ}\text{C}$ . Where indicated, cultures were treated basally with 50 ng/ml IFN- $\text{L1}$  (Peprotech) at the indicated time pre- or post-infection. Prior to determining the viral titer, all samples were centrifuged at 2,000 g for 5 min. Infectious virus titers were determined using the Spearman & Kärber TCID<sub>50</sub> method on VeroE6 cells. All work was performed in a Class II Biosafety Cabinet under BSL-3 conditions at Erasmus Medical Center.

### Fixed immunofluorescence microscopy

Organoids and Transwell inserts were fixed in 4% paraformaldehyde for 20 min, permeabilized in 70% ethanol or 0.1% Triton X-100 in PBS, and blocked for 60 min in 10% normal goat serum or 3% bovine serum albumin (BSA) in PBS (blocking buffer). For organoids, 0.1% Triton X-100 was added to the blocking buffer to increase antibody penetration. Cells were incubated with primary antibodies overnight at  $4^{\circ}\text{C}$  in blocking buffer, washed twice with PBS, incubated with corresponding secondary antibodies Alexa 488- and Alexa 594-conjugated secondary antibodies (1:200; Invitrogen) in blocking buffer for 2 h at room temperature, washed two times with PBS, incubated with indicated additional stains (TO-PRO3, phalloidin-633 (Santa Cruz, sc-363796), Hoechst, DAPI), washed twice with PBS, and mounted in Prolong Antifade (Invitrogen) mounting medium.

Viral nucleocapsid was stained with mouse-anti-SARS-CoV NP (40143-MM05, 1:1,000, Sino Biological) or rabbit-anti-SARS-CoV NP (40143-T62, 1:1,000, Sino biological), alveolar type 2 cells with anti-HTII-280 (TB-27AHT2-280, 1:150, Terrace Biotech), anti-SFTPC (FL-197, 1:200, Santa Cruz), anti-LPCAT1 (HPA012501, 1:200, Sigma), alveolar type 1 cells with anti-HTI-56 (TB-29 AHTI-56, 1:30, Terrace Biotech) and anti-HOPX (sc-30216, 1:200, Santa Cruz Biotechnology), goblet cells with anti-MUC5AC (MA5-12178, 1:100, Invitrogen), club cells with anti-CC10 (sc-390313 AF594, 1:100, Santa Cruz

Biotechnology) or anti-SCGB3A2 (AF3545, 1:100, R&D systems), ciliated cells with anti-AcTUB (sc-23950 AF488, 1:100, Santa Cruz Biotechnology), STAT1 translocation anti-pSTAT1 (MA5-15071, 1:100, Thermo Fisher), proliferating cells with anti-Ki67 (MIB-1, GAG2661-2, 1:100, DAKO), tight junctions with anti-ZO-1 (ZO1-1A12, 1:100, Invitrogen), multipotent lung bud tip stem cells with anti-SOX2 (sc-365823 AF488, 1:100, Santa Cruz Biotechnology) and anti-SOX9 (sc-166505 AF594, 1:100, Santa Cruz Biotechnology), basal cells with anti-TP63 (ab735, 1:500, Abcam), and pulmonary neuroendocrine cells with anti-SYP (sc-17750, 1:100, Santa Cruz Biotechnology). ACE2 was stained with anti-ACE2 (HPA000288, 1:200, Atlas antibodies), and TMPRSS2 was stained with anti-TMPRSS2 (sc-515727, 1:200, Santa Cruz). Samples were imaged on a LSM700 confocal microscope using ZEN software (Zeiss). Representative images were acquired and shown as Z-projections, single slices or XZ cross sections.

### Procurement of human material and informed consent

Adult lung tissue was obtained from residual, tumor-free, material obtained at lung resection surgery for lung cancer. The Medical Ethical Committee of the Erasmus MC Rotterdam granted permission for this study (METC 2012-512). Human fetal lung tissue was obtained from legally terminated second trimester pregnancies (15–20 weeks) by the HIS-Mouse Facility of Academic Medical Center (AMC; Amsterdam, The Netherlands), after written informed consent of the mother for the tissue's use in research and with approval of the Medical Ethical Review Board of the AMC (MEC: 03/038). Study procedures were performed according to the Declaration of Helsinki, and in compliance with relevant Dutch laws and institutional guidelines. The tissues obtained were anonymized and non-traceable to the donor. On request by the researchers, only gender and gestational age is provided.

### Isolation, culture, and differentiation of human small airway stem cells

Isolation of human small airway stem cells was performed using a protocol adapted from Sachs *et al* (2019). One adult small airway donor was used in this study. Distal regions of adult lungs (lung parenchyma) were cut into  $\sim 2$  mm sections, washed in AdDF++, and incubated with dispase (Corning; #354235) mixed with airway organoid (AO) medium (Sachs *et al*, 2019) at a 1:1 ratio for 1 h at  $37^{\circ}\text{C}$ . The digested tissue suspension was sequentially sheared using 10- and 5-ml plastic and flamed glass Pasteur pipettes. After shearing, the suspension was strained over a 100- $\mu\text{m}$  filter. Two percent FCS was added to the strained suspension before centrifugation at 400 g. The pellet was resuspended in 10 ml AdDF+++ and centrifuged again at 400 g. In case of a visible red pellet, erythrocytes were lysed in 2 ml red blood cell lysis buffer (Roche-11814389001) for 5 min at room temperature before the addition of 10 ml AdDF+++ and centrifugation at 400 g. Lung cell pellets were then resuspended in 200  $\mu\text{l}$  of growth factor reduced Matrigel (Corning; #356231) and plated in  $\sim 30$   $\mu\text{l}$  droplets in a 48-well tissue culture plate. Plates were placed at  $37^{\circ}\text{C}$  with 5% CO<sub>2</sub> for 10 min to solidify the Matrigel droplets upon which 250  $\mu\text{l}$  of media was added to each well. Plates were incubated under standard tissue culture conditions ( $37^{\circ}\text{C}$ , 5% CO<sub>2</sub>).

Airway organoids were passaged by mechanical disruption at 1:2 to 1:4 ratios after 10–14 days of culture. Medium was aspirated and

ice-cold AdDF+++ added to each well. The Matrigel in each well was disrupted by pipetting and sucked into a P1000 pipette tip and transferred into a 15-ml tube. Ice-cold AdDF+++ was added up to 10 ml after which the sample was centrifuged at 100 g for 5 min. The medium was aspirated and replaced by 1 ml TrypLE express (Gibco). Next, organoids were incubated at 37°C for 5 min after which they were triturated using a flame-polished glass Pasteur pipette. Cold AdDF+++ containing 2% FCS was added up to 10 ml, and the sample was centrifuged at 400 g for 3 min. Medium was aspirated, washed once in cold AdDF+++ and the pellet incubated on ice for 2 min before being resuspended in Matrigel and plated in ~30 µl droplets in a 48-well tissue culture. Plates were placed at 37°C with 5% CO<sub>2</sub> for 20 min to solidify the Matrigel droplets, upon which 250 µl AO medium was added per well. Medium was changed every 4 days.

To obtain differentiated organoid-derived cultures, organoids were dissociated into single cells using TrypLE express. Cells were seeded on Transwell membranes (Corning) coated with rat tail collagen type I (Fisher Scientific). Single cells were seeded in AO growth medium:complete base medium (CBM; Stemcell Pneumacult-ALI; #05001) at a 1:1 ratio. After 2–4 days, confluent monolayers were cultured at air–liquid interface in CBM. Medium was changed every 5 days. After 8 weeks of differentiation, cultures were used for infection experiments.

#### Isolation, culture, and differentiation of human fetal lung bud tips

Isolation of human fetal lung epithelial bud tips was performed using a protocol adapted from Miller *et al* (2018). Fetal lung donors were 16–19 weeks post-conception (pcw). Tissues were shipped in Hibernate A (Gibco; #A1247501) on ice before processing on the day the specimen was obtained. Distal regions of fetal lungs were cut into ~2 mm sections and incubated with dispase on ice for 30–60 min. Tissue pieces were then incubated in 100% FBS on ice for 15 min, after which they were transferred to a 10% FBS solution in AdDF++. Lung bud tips were separated from mesenchymal cells through repeated pipetting and washing in AdDF++ until mesenchymal cells were no longer visible. From each donor, donor-specific mesenchymal cells were isolated by plating single cells present in the supernatant from the first wash. Mesenchymal cells were maintained in AdDF++ supplemented with 10% FCS. After washing, bud tips were then resuspended in 200 µl of growth factor reduced Matrigel and plated in ~30 µl droplets in a 48-well tissue culture plate. Plates were placed at 37°C with 5% CO<sub>2</sub> for 20 min to solidify the Matrigel droplets upon which 250 µl of fetal lung (FL) medium (Nikolic *et al*, 2017) was added to each well. Plates were incubated under standard tissue culture conditions (37°C, 5% CO<sub>2</sub>).

Fetal lung bud tip organoids were passaged by mechanical disruption at 1:2 to 1:4 ratios after 10–14 days of culture. Medium was aspirated and ice-cold AdDF+++ added to each well. The Matrigel in each well was disrupted by pipetting and sucked into a P1000 pipette tip and transferred into a 15-ml tube. Ice-cold AdDF+++ was added up to 10 ml after which the sample was centrifuged at 100 g for 5 min. The medium was aspirated and replaced by 1 ml AdDF++. Next, organoids were triturated using a flame-polished glass Pasteur pipette. Cold AdDF+++ was added up to 10 ml, and the sample was centrifuged at 400 g for 3 min. Medium was aspirated and the pellet incubated on ice for 2 min before being resuspended in Matrigel and plated in ~30 µl droplets in a 48-well

tissue culture. Plates were placed at 37°C with 5% CO<sub>2</sub> for 20 min to solidify the Matrigel droplets, upon which 250 µl FL medium was added per well. Medium was changed every 4 days.

To obtain differentiated organoid-derived cultures, 10<sup>5</sup> donor-specific fetal lung mesenchymal cells were seeded in 12-well plates in AdDF+++ containing 10% FCS. The next day, organoids were dissociated into small clumps using TrypLE express. Cells were seeded on Transwell membranes (Corning-3460). Clumps were seeded in FL:BEpiCM (bronchial epithelial cell growth medium; Sciencell; Cat. No. 3211) at a 1:1 ratio. BEpiCM was made by mixing basal medium (Sciencell; Cat. No. 3211-b) and DMEM at a 1:1 ratio and adding bronchial epithelial cell growth supplement (BEpiCGS, Sciencell; Cat. No. 3262), penicillin (100 IU/ml), streptomycin (100 IU/ml), and 0.001 µM retinoic acid (Sigma). ROCK inhibitor was added for the first 5 days to prevent apoptosis (Y-27632; Sigma; Y0503; 10 µM). After 4–7 days, confluent monolayers were cultured at air–liquid interface in BEpiCM. Eighty percent of the medium was changed every 4–5 days. After 14 days of differentiation, cultures were used for infection experiments.

#### Determination of virus titers using qRT-PCR

Supernatant and organoid samples were thawed and centrifuged at 2,000 g for 5 min. Sixty µl supernatant was lysed in 90 µl MagnaPure LC Lysis buffer (Roche) at room temperature for 10 min. RNA was extracted by incubating samples with 50 µl Agencourt AMPure XP beads (Beckman Coulter) for 15 min at RT, washing beads twice with 70% ethanol on a DynaMag-96 magnet (Invitrogen), and eluting in 30 µl MagnaPure LC elution buffer (Roche). Viral titers (Viral RNA copies per ml) were determined by qRT-PCR using primers targeting the E gene (35) and compared to a counted RNA standard curve.

#### Mass spectrometry

Proteins were digested with trypsin using the SP3 method (Hughes *et al*, 2019) with minor modifications. Briefly, proteins secreted by alveolar-like cultures were collected from the cells by adding 200 µl AdDF+++ apically, incubating 10 min at 37°C 5% CO<sub>2</sub>, and storing the supernatant at –80°C in Laemmli buffer (Bio-Rad). Proteins in 30 µl Laemmli buffer (Bio-Rad) were reduced with 5 mM dithiothreitol (Sigma, D8255) for 30 min at 50°C and alkylated with 10 mM iodoacetamide (Sigma, I6125) for 10 min in the dark. Ten µg Sera-Mag SpeedBeads (Fisher Scientific) in 20 µl milli-Q and ethanol were added to a final concentration of 50%, and the solution was mixed for 10 min at RT. Beads were immobilized using a magnetic rack and washed three times with 100 µl 80% ethanol. One 1 µg trypsin and 0.5 µg Lys-C in 100 µl 50 mM Tris/HCl pH 8.3 were added to the beads, and the sample was incubated overnight at 37°C. The tryptic digest was acidified with TFA and desalted using a StageTip. Peptides were eluted with 100 µl 40% Acetonitrile and 0.1% formic acid and dried in a Speedvac. Before analysis by LC-MS, peptides were dissolved in 20 µl 2% acetonitrile and 0.1% formic acid.

Nanoflow liquid chromatography–tandem mass spectrometry (nLC-MS/MS) was performed on an EASY-nLC 1200 coupled to an Orbitrap Eclipse Tribrid mass spectrometer (Thermo Fisher Scientific) operating in positive mode. Peptide mixtures were trapped on a 2 cm × 100 µm Pepmap C18 column (Thermo Fisher 164564) and then separated on an in-house packed 50 cm × 75 µm capillary column with 1.9 µm Reprosil-Pur C18 beads (Dr. Maisch) at a

flowrate of 250 nL/min, using a linear gradient of 0–32% acetonitrile (in 0.1% formic acid) during 90 min. The eluate was directly sprayed into the electrospray ionization (ESI) source of the mass spectrometer. Spectra were acquired in continuum mode; fragmentation of the peptides was performed in data-dependent mode by HCD. Mass spectrometry data were analyzed with Proteome Discoverer 2.4 with Mascot version 2.6.2 as the search engine. The target FDR for both PSMs and peptides was set to 0.01. MS/MS spectra were searched against a combined database composed of all UniProt entries taxonomy *Homo Sapiens* (release October 2019) and all SARS-CoV-2 protein sequences (<https://covid-19.uniprot.org/>) concatenated with the reversed versions of all sequences. For precursor ion quantification based on the Minora algorithm in Proteome Discoverer, only unique and razor peptides were used. Normalization was done on total peptide amounts for all samples.

### Bulk RNA sequencing

Library preparation was performed at Single Cell Discoveries (Utrecht, The Netherlands), using an adapted version of the CEL-seq protocol. In brief:

Total RNA was extracted using the standard TRIzol (Invitrogen) protocol and used for library preparation and sequencing. mRNA was processed as described previously, following an adapted version of the single-cell mRNA seq protocol of CEL-Seq (Simmini *et al*, 2014; Hashimshony *et al*, 2016). In brief, samples were barcoded with CEL-seq primers during a reverse transcription and pooled after second strand synthesis. The resulting cDNA was amplified with an overnight *in vitro* transcription reaction. From this amplified RNA, sequencing libraries were prepared with Illumina TruSeq small RNA primers. Paired-end sequencing was performed on the Illumina NextSeq 500 platform using barcoded 1 × 75 nt read setup. Read 1 was used to identify the Illumina library index and CEL-Seq sample barcode. Read 2 was aligned to the CRCh38 human RefSeq transcriptome, with the addition of the SARS-CoV-2 (Ref-SKU: 026V-03883) genome, similar to earlier study (Lamers *et al*, 2020), using BWA using standard settings (Li & Durbin, 2010). Reads that mapped equally well to multiple locations were discarded. Mapping and generation of count tables was done using the MapAndGo script. Samples were normalized using RPM normalization.

Differential gene expression analysis was performed using the DESeq2 package (Love *et al*, 2014). SARS-mapping reads were removed before analyzing the different datasets.

For bronchioalveolar-like samples, two donors were sequenced twice as technical replicates which were combined in the DESeq2 methods when comparing to the remaining datasets. We compared the bulk mRNA sequencing of the bronchioalveolar culture system to freshly purified adult ATII cells. Previously published profiles of purified human ATII cultures were downloaded from NCBI GEO (Accession Nos. GSM3818009 and GSM3818010). Normalized counts were used in generating heatmaps.

The top genes which were most strongly induced in response to SARS-CoV-2 ( $P_{adj} < 0.05$ , ranked by fold change) were subjected to functional enrichment analysis for a biological process using ToppFun on the ToppGene Suite (<https://toppgene.cchmc.org/enrichment.jsp>) as described before (Kaimal *et al*, 2010). The five biological processes with highest enrichment (after FDR correction and a  $P$ -value cutoff of 0.05) for each virus are displayed with the corresponding GO term, corrected  $P$ -value, and FDR.

### 10× Single-cell sequencing—library preparation

Single-cell mRNA sequencing was performed at Single Cell Discoveries according to standard 10× Genomics 3' V3.1 chemistry protocol. In short, single-cell suspensions were methanol fixed in 80% methanol and frozen at  $-80^{\circ}\text{C}$ . Prior to loading the cells on the 10× Chromium controller, cells were rehydrated in rehydration buffer and counted to assess cell concentration. Cells were loaded, and the resulting sequencing libraries were prepared following standard 10× Genomics protocol. The DNA libraries were paired-end sequenced on an Illumina NovaSeq S4, with a  $2 \times 150$  bp Illumina kit.

### 10× Single-cell sequencing—Mapping of sequencing data and clustering and differential gene expression analysis

BCL files resulting from sequencing were transformed to FASTQ files with 10× Genomics Cell Ranger mkfastq. FASTQ files were mapped with Cell Ranger count. During sequencing, Read 1 was assigned 150 base pairs, but only the first 28 bp were used for identification of the Illumina library barcode, cell barcode, and UMI. R2 was used to map to a custom made reference transcriptome of Hg38 with additional sequences for SARS-CoV-2 added. Filtering of empty barcodes was done Cell Ranger. In total, approximately 5,015 cells were detected. Unsupervised clustering and differential gene expression analysis was done with the Seurat<sup>1</sup> R toolkit (Butler *et al*, 2018). We compared the ATII-L cells in the bronchioalveolar culture system to purified ATII cells. Previously published single-cell transcriptomic profiles of purified ATII cultures were downloaded from NCBI GEO (Accession No GSM2855485). Raw counts were normalized, integrated with the abovementioned single-cell dataset, and further analyzed using the Seurat R toolkit.

### Transmission electron microscopy

2D cultures were chemically fixed for 3 h at room temperature and prepared for imaging within the transmission electron microscope as described in (Lamers *et al*, 2020). All TEM data were collected with an Eagle detector on a FEI Tecnai T12 microscope operated at 120 kV.

### Statistical analysis

For single-cell sequencing data, clustering and differential gene expression analysis was performed with Seurat version 3 (Butler *et al*, 2018), following standard parameters.

## Data availability

Bulk RNA and 10× single-cell RNA sequencing data are deposited at Gene Expression Omnibus under GSE153218 (<http://www.ncbi.nlm.nih.gov/geo/query/acc.cgi?acc=GSE153218>) and GSE161934 (<http://www.ncbi.nlm.nih.gov/geo/query/acc.cgi?acc=GSE161934>), respectively.

**Expanded View** for this article is available online.

### Acknowledgements

We thank A de Graaff and Hubrecht Imaging Centre (HIC) for microscopy assistance and Single Cell Discoveries for single-cell sequencing and mRNA library preparation, and the Utrecht Sequencing Facility (subsidized by the University Medical Center Utrecht, Hubrecht Institute, Utrecht University and NWO



project 184.034.019). KK, PJP, and RBGR received funding from the Dutch Technology Foundation STW under project name UPON, number 14207. We acknowledge the Maastricht M4I Microscopy CORE Lab for their scientific and technological support. This work was supported by NWO Grant 022.005.032. We thank Evelien Eenjes and Robbert Rottier for providing human adult lung material.

### Author contributions

Conceptualization, MML, JvdV, JB, HC, BLH; Methodology, MML, JVDV, KK, SR, JAAD, MJM, PJP, HC, BLH; Investigation, MML, JvdV, KK, SR, TIB, AZM, DS, KB, CDK, NG, RBGR, HQD, JAAD; Resources, GMGMV, MPKG, HC; Writing-Original Draft, MML, JVDV, BLH; Writing-Review & Editing, PJP, HC, BLH; Funding acquisition, PJP, HC, BLH.

### Conflict of interest

H.C. is inventor on patents held by the Royal Netherlands Academy of Arts and Sciences that cover organoid technology. H.C.'s full disclosure is given at <https://www.uu.nl/staff/JCClevers/>.

## References

- Ackermann M, Verleden SE, Kuehnel M, Haverich A, Welte T, Laenger F, Vanstapel A, Werlein C, Stark H, Tzankov A et al (2020) Pulmonary vascular endothelialitis, thrombosis, and angiogenesis in Covid-19. *N Engl J Med* 383: 120–128
- Andersen KG, Rambaut A, Lipkin WI, Holmes EC, Garry RF (2020) The proximal origin of SARS-CoV-2. *Nat Med* 26: 450–452
- Barkauskas CE, Counce MJ, Rackley CR, Bowie EJ, Keene DR, Stripp BR, Randell SH, Noble PW, Hogan BL (2013) Type 2 alveolar cells are stem cells in adult lung. *J Clin Invest* 123: 3025–3036
- Barton LM, Duval EJ, Stroberg E, Ghosh S, Mukhopadhyay S (2020) COVID-19 autopsies, Oklahoma, USA. *Am J Clin Pathol* 153: 725–733
- Blanco-Melo D, Nilsson-Payant BE, Liu WC, Uhl S, Hoagland D, Moller R, Jordan TX, Oishi K, Panis M, Sachs D et al (2020) Imbalanced host response to SARS-CoV-2 drives development of COVID-19. *Cell* 181: 1036–1045
- Butler A, Hoffman P, Smibert P, Papalexi E, Satija R (2018) Integrating single-cell transcriptomic data across different conditions, technologies, and species. *Nat Biotechnol* 36: 411–420
- Chen N, Zhou M, Dong X, Qu J, Gong F, Han Y, Qiu Y, Wang J, Liu Y, Wei Y et al (2020) Epidemiological and clinical characteristics of 99 cases of 2019 novel coronavirus pneumonia in Wuhan, China: a descriptive study. *Lancet* 395: 507–513
- Coronaviridae Study Group of the International Committee on Taxonomy of V (2020) The species Severe acute respiratory syndrome-related coronavirus: classifying 2019-nCoV and naming it SARS-CoV-2. *Nat Microbiol* 5: 536–544
- Corman VM, Landt O, Kaiser M, Molenkamp R, Meijer A, Chu DK, Bleicker T, Brunink S, Schneider J, Surveill ML et al (2020) Detection of 2019 novel coronavirus (2019-nCoV) by real-time RT-PCR. *Euro Surveill* 25: 2000045
- de Carvalho A, Strikoudis A, Liu HY, Chen YW, Dantas TJ, Vallee RB, Correia-Pinto J, Snoeck HW (2019) Glycogen synthase kinase 3 induces multilineage maturation of human pluripotent stem cell-derived lung progenitors in 3D culture. *Development* 146: dev171652
- Dobbs LG, Gonzalez RF, Allen L, Froh DK (1999) HTI56, an integral membrane protein specific to human alveolar type I cells. *J Histochem Cytochem* 47: 129–137
- Dye BR, Hill DR, Ferguson MA, Tsai YH, Nagy MS, Dyal R, Wells JM, Mayhew CN, Nattiv R, Klein OD et al (2015) *In vitro* generation of human pluripotent stem cell derived lung organoids. *Elife* 4: e05098
- Frieman M, Yount B, Heise M, Kopecky-Bromberg SA, Palese P, Baric RS (2007) Severe acute respiratory syndrome coronavirus ORF6 antagonizes STAT1 function by sequestering nuclear import factors on the rough endoplasmic reticulum/Golgi membrane. *J Virol* 81: 9812–9824
- Gonzales LW, Gonzalez R, Barrette AM, Wang P, Dobbs L, Ballard PL (2015) Expression of carcinoembryonic cell adhesion molecule 6 and alveolar epithelial cell markers in lungs of human infants with chronic lung disease. *J Histochem Cytochem* 63: 908–921
- Gonzalez RF, Allen L, Gonzales L, Ballard PL, Dobbs LG (2010) HTII-280, a biomarker specific to the apical plasma membrane of human lung alveolar type II cells. *J Histochem Cytochem* 58: 891–901
- Gotoh S, Ito I, Nagasaki T, Yamamoto Y, Konishi S, Korogi Y, Matsumoto H, Muro S, Hirai T, Funato M et al (2014) Generation of alveolar epithelial spheroids via isolated progenitor cells from human pluripotent stem cells. *Stem Cell Reports* 3: 394–403
- Hashimshony T, Senderovich N, Avital G, Klochendler A, de Leeuw Y, Anavy L, Gennert D, Li S, Livak KJ, Rozenblatt-Rosen O et al (2016) CEL-Seq2: sensitive highly-multiplexed single-cell RNA-Seq. *Genome Biol* 17: 77
- Hikmet F, Mear L, Edvinsson A, Micke P, Uhlen M, Lindskog C (2020) The protein expression profile of ACE2 in human tissues. *Mol Syst Biol* 16: e9610
- Hoffmann M, Kleine-Weber H, Schroeder S, Kruger N, Herrler T, Erichsen S, Schiergens TS, Herrler G, Wu NH, Nitsche A et al (2020) SARS-CoV-2 cell entry depends on ACE2 and TMPRSS2 and is blocked by a clinically proven protease inhibitor. *Cell* 181: 271–280
- Hou YJ, Okuda K, Edwards CE, Martinez DR, Asakura T, Dinno III KH, Kato T, Lee RE, Yount BL, Mascenik TM et al (2020) SARS-CoV-2 reverse genetics reveals a variable infection gradient in the respiratory tract. *Cell* 182: 429–446
- Huang J, Hume AJ, Abo KM, Werder RB, Villacorta-Martin C, Alysandratos KD, Beermann ML, Simone-Roach C, Lindstrom-Vautrin J, Olejnik J et al (2020) SARS-CoV-2 infection of pluripotent stem cell-derived human lung alveolar type 2 cells elicits a rapid epithelial-intrinsic inflammatory response. *Cell Stem Cell* 27: 962–973
- Hughes CS, Moggridge S, Muller T, Sorensen PH, Morin GB, Krijgsveld J (2019) Single-pot, solid-phase-enhanced sample preparation for proteomics experiments. *Nat Protoc* 14: 68–85
- Hui KPY, Cheung MC, Perera R, Ng KC, Bui CHT, Ho JCW, Ng MMT, Kuok DIT, Shih KC, Tsao SW et al (2020) Tropism, replication competence, and innate immune responses of the coronavirus SARS-CoV-2 in human respiratory tract and conjunctiva: an analysis in *ex-vivo* and *in-vitro* cultures. *Lancet Respir Med* 8: 687–695
- Jacob A, Morley M, Hawkins F, McCauley KB, Jean JC, Heins H, Na CL, Weaver TE, Vedaie M, Hurley K et al (2017) Differentiation of human pluripotent stem cells into functional lung alveolar epithelial cells. *Cell Stem Cell* 21: 472–488
- Jia HP, Look DC, Shi L, Hickey M, Pewe L, Netland J, Farzan M, Wohlford-Lenane C, Perlman S, McCray Jr PB (2005) ACE2 receptor expression and severe acute respiratory syndrome coronavirus infection depend on differentiation of human airway epithelia. *J Virol* 79: 14614–14621
- Kaimal V, Bardes EE, Tabar SC, Jegga AG, Aronow BJ (2010) ToppCluster: a multiple gene list feature analyzer for comparative enrichment clustering and network-based dissection of biological systems. *Nucleic Acids Res* 38: W96–W102

- Katsura H, Sontake V, Tata A, Kobayashi Y, Edwards CE, Heaton BE, Konkimalla A, Asakura T, Mikami Y, Fritch EJ *et al* (2020) Human lung stem cell-based alveolospheres provide insights into SARS-CoV-2-mediated interferon responses and pneumocyte dysfunction. *Cell Stem Cell* 27: 890–904.
- Kim CF, Jackson EL, Woolfenden AE, Lawrence S, Babar I, Vogel S, Crowley D, Bronson RT, Jacks T (2005) Identification of bronchioalveolar stem cells in normal lung and lung cancer. *Cell* 121: 823–835
- Kopecky-Bromberg SA, Martinez-Sobrido L, Frieman M, Baric RA, Palese P (2007) Severe acute respiratory syndrome coronavirus open reading frame (ORF) 3b, ORF 6, and nucleocapsid proteins function as interferon antagonists. *J Virol* 81: 548–557
- Lamers MM, Beumer J, van der Vaart J, Knoops K, Puschhof J, Breugem TI, Ravelli RBG, Paul van Schayck J, Mykityn AZ, Duimel HQ *et al* (2020) SARS-CoV-2 productively infects human gut enterocytes. *Science* 369: 50–54
- Lauer SA, Grantz KH, Bi Q, Jones FK, Zheng Q, Meredith HR, Azman AS, Reich NG, Lessler J (2020) The incubation period of coronavirus disease 2019 (COVID-19) from publicly reported confirmed cases: estimation and application. *Ann Intern Med* 172: 577–582
- Leeman KT, Pessina P, Lee JH, Kim CF (2019) Mesenchymal stem cells increase alveolar differentiation in lung progenitor organoid cultures. *Sci Rep* 9: 6479
- Li H, Durbin R (2010) Fast and accurate long-read alignment with Burrows-Wheeler transform. *Bioinformatics* 26: 589–595
- Logan CY, Desai TJ (2015) Keeping it together: Pulmonary alveoli are maintained by a hierarchy of cellular programs. *BioEssays* 37: 1028–1037
- Love MI, Huber W, Anders S (2014) Moderated estimation of fold change and dispersion for RNA-seq data with DESeq2. *Genome Biol* 15: 550
- Lu R, Zhao X, Li J, Niu P, Yang B, Wu H, Wang W, Song H, Huang B, Zhu N *et al* (2020) Genomic characterisation and epidemiology of 2019 novel coronavirus: implications for virus origins and receptor binding. *Lancet* 395: 565–574
- Menter T, Haslbauer JD, Nienhold R, Savic S, Hopfer H, Deigendesch N, Frank S, Turek D, Willi N, Pargger H *et al* (2020) Post-mortem examination of COVID-19 patients reveals diffuse alveolar damage with severe capillary congestion and variegated findings of lungs and other organs suggesting vascular dysfunction. *Histopathology* 77: 198–209
- Miller AJ, Hill DR, Nagy MS, Aoki Y, Dye BR, Chin AM, Huang S, Zhu F, White ES, Lama V *et al* (2018) In vitro induction and in vivo engraftment of lung bud tip progenitor cells derived from human pluripotent stem cells. *Stem Cell Rep* 10: 101–119
- Mu J, Fang Y, Yang Q, Shu T, Wang A, Huang M, Jin L, Deng F, Qiu Y, Zhou X (2020) SARS-CoV-2 N protein antagonizes type I interferon signaling by suppressing phosphorylation and nuclear translocation of STAT1 and STAT2. *Cell Discov* 6: 65
- Nikolic MZ, Carigt O, Jeng Q, Johnson JA, Sun D, Howell KJ, Brady JL, Laresgoiti U, Allen G, Butler R *et al* (2017) Human embryonic lung epithelial tips are multipotent progenitors that can be expanded *in vitro* as long-term self-renewing organoids. *Elife* 6: e26575
- Nikolic MZ, Rawlins EL (2017) Lung organoids and their use to study cell-cell interaction. *Curr Pathobiol Rep* 5: 223–231
- Qi F, Qian S, Zhang S, Zhang Z (2020) Single cell RNA sequencing of 13 human tissues identify cell types and receptors of human coronaviruses. *Biochem Biophys Res Commun* 526: 135–140
- Raptis CA, Hammer MM, Short RG, Shah A, Bhalla S, Bierhals AJ, Filev PD, Hope MD, Jeudy J, Kligerman SJ *et al* (2020) Chest CT and coronavirus disease (COVID-19): a critical review of the literature to date. *AJR Am J Roentgenol* 215: 839–842
- Ravindra NG, Alfajaro MM, Gasque V, Wei J, Filler RB, Huston NC, Wan H, Szigeti-Buck K, Wang B, Montgomery RR *et al* (2020) Single-cell longitudinal analysis of SARS-CoV-2 infection in human bronchial epithelial cells. *bioRxiv* <https://doi.org/10.1101/2020.05.06.081695> [PREPRINT]
- Rockx B, Kuiken T, Herfst S, Bestebroer T, Lamers MM, Oude Munnink BB, de Meulder D, van Amerongen G, van den Brand J, Okba NMA *et al* (2020) Comparative pathogenesis of COVID-19, MERS, and SARS in a nonhuman primate model. *Science* 368: 1012–1015
- Sachs N, Papaspyropoulos A, Zomer-van Ommen DD, Heo I, Bottinger L, Klay D, Weeber F, Huelsz-Prince G, Iakobachvili N, Amatngalim GD *et al* (2019) Long-term expanding human airway organoids for disease modeling. *EMBO J* 38: e100300
- Salahudeen AA, Choi SS, Rustagi A, Zhu J, van Unen V, de la O SM, Flynn RA, Margalef-Catala M, Santos AJM, Ju J *et al* (2020) Progenitor identification and SARS-CoV-2 infection in human distal lung organoids. *Nature* <https://doi.org/10.1038/s41586-020-3014-1>
- Simmini S, Bialecka M, Huch M, Kester L, van de Wetering M, Sato T, Beck F, van Oudenaarden A, Clevers H, Deschamps J (2014) Transformation of intestinal stem cells into gastric stem cells on loss of transcription factor Cdx2. *Nat Commun* 5: 5728
- tenOever BR (2016) The evolution of antiviral defense systems. *Cell Host Microbe* 19: 142–149
- Thompson BT, Chambers RC, Liu KD (2017) Acute respiratory distress syndrome. *N Engl J Med* 377: 562–572
- van den Bogaard EH, Dailey LA, Thorley AJ, Tetley TD, Forbes B (2009) Inflammatory response and barrier properties of a new alveolar type 1-like cell line (TT1). *Pharm Res* 26: 1172–1180
- van den Brink SC, Sage F, Vértessy Á, Spanjaard B, Peterson-Maduro J, Baron CS, Robin C, van Oudenaarden A (2017) Single-cell sequencing reveals dissociation-induced gene expression in tissue subpopulations. *Nat Methods* 14: 935–936
- van den Riet S, Ninaber DK, Mikkers HMM, Tetley TD, Jost CR, Mulder AA, Pasman T, Baptista D, Poot AA, Truckenmuller R *et al* (2020) *In vitro* modelling of alveolar repair at the air-liquid interface using alveolar epithelial cells derived from human induced pluripotent stem cells. *Sci Rep* 10: 5499
- Walls AC, Park YJ, Tortorici MA, Wall A, McGuire AT, Veesler D (2020) Structure, function, and antigenicity of the SARS-CoV-2 spike glycoprotein. *Cell* 181: 281–292
- Wang D, Hu B, Hu C, Zhu F, Liu X, Zhang J, Wang B, Xiang H, Cheng Z, Xiong Y *et al* (2020) Clinical characteristics of 138 hospitalized patients with 2019 novel coronavirus-infected pneumonia in Wuhan, China. *JAMA* 323: 1061
- Ware LB, Matthay MA (2000) The acute respiratory distress syndrome. *N Engl J Med* 342: 1334–1349
- WHO (2020) Coronavirus disease (COVID-19). Situation Report – 132
- Wolfel R, Corman VM, Guggemos W, Seilmaier M, Zange S, Muller MA, Niemeyer D, Jones TC, Vollmar P, Rothe C *et al* (2020) Virological assessment of hospitalized patients with COVID-2019. *Nature* 581: 465–469
- Wrapp D, Wang N, Corbett KS, Goldsmith JA, Hsieh CL, Abiona O, Graham BS, McLellan JS (2020) Cryo-EM structure of the 2019-nCoV spike in the prefusion conformation. *Science* 367: 1260–1263
- Xu Z, Shi L, Wang Y, Zhang J, Huang L, Zhang C, Liu S, Zhao P, Liu H, Zhu L *et al* (2020) Pathological findings of COVID-19 associated with acute respiratory distress syndrome. *Lancet Respir Med* 8: 420–422
- Yamamoto Y, Gotoh S, Korogi Y, Seki M, Konishi S, Ikey S, Sone N, Nagasaki T, Matsumoto H, Muro S *et al* (2017) Long-term expansion of alveolar stem

- cells derived from human iPS cells in organoids. *Nat Methods* 14: 1097–1106
- Youk J, Kim T, Evans KV, Jeong YI, Hur Y, Hong SP, Kim JH, Yi K, Kim SY, Na KJ *et al* (2020) Three-dimensional human alveolar stem cell culture models reveal infection response to SARS-CoV-2. *Cell Stem Cell* 27: 905–919
- Zacharias WJ, Frank DB, Zepp JA, Morley MP, Alkhaleel FA, Kong J, Zhou S, Cantu E, Morrissey EE (2018) Regeneration of the lung alveolus by an evolutionarily conserved epithelial progenitor. *Nature* 555: 251–255
- Zhou J, Li C, Sachs N, Chiu MC, Wong BH, Chu H, Poon VK, Wang D, Zhao X, Wen L *et al* (2018) Differentiated human airway organoids to assess infectivity of emerging influenza virus. *Proc Natl Acad Sci USA* 115: 6822–6827
- Zhou P, Yang XL, Wang XG, Hu B, Zhang L, Zhang W, Si HR, Zhu Y, Li B, Huang CL *et al* (2020) A pneumonia outbreak associated with a new coronavirus of probable bat origin. *Nature* 579: 270–273
- Zhu N, Zhang D, Wang W, Li X, Yang B, Song J, Zhao X, Huang B, Shi W, Lu R *et al* (2020) A novel coronavirus from patients with pneumonia in China, 2019. *N Engl J Med* 382: 727–733
- Ziegler CGK, Allon SJ, Nyquist SK, Mbano IM, Miao VN, Tzouanas CN, Cao Y, Yousif AS, Bals J, Hauser BM *et al* (2020) SARS-CoV-2 receptor ACE2 is an interferon-stimulated gene in human airway epithelial cells and is detected in specific cell subsets across tissues. *Cell* 181: 1016–1035



**License:** This is an open access article under the terms of the Creative Commons Attribution-NonCommercial-NoDerivs 4.0 License, which permits use and distribution in any medium, provided the original work is properly cited, the use is non-commercial and no modifications or adaptations are made.